iScience

CellPress
OPEN ACCESS

Article

Semaphorin3E-PlexinD1 signaling in coronary artery and lymphatic vessel development with clinical implications in myocardial recovery

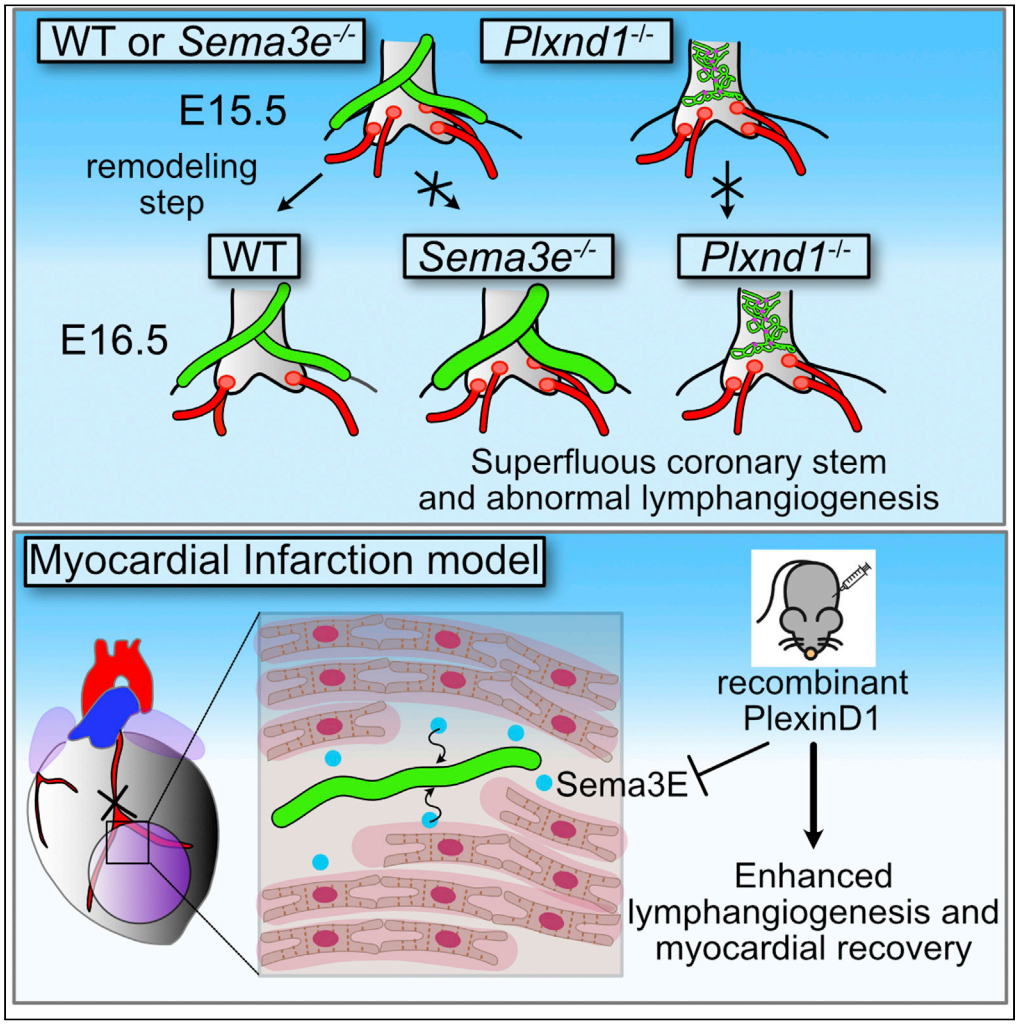

Kazuaki Maruyama, Kazuaki Naemura, Yuichiro Arima, ..., Yukiko Kurihara, Sachiko Miyagawa-Tomita, Hiroki Kurihara

k.maruyama0608@gmail.com (K.M.)
kuri-tky@umin.net (H.K.)

Highlights

Sema3E-PlexinD1 signaling regulates coronary and cardiac lymphatic vessel development

Sema3E demarcate areas to repel PlexinD1-expressing lymphatic endothelial cells

Inhibition of Sema3E-PlexinD1 signaling improves the recovery after myocardial injury

Maruyama et al., iScience 24, 102305
April 23, 2021
https://doi.org/10.1016/j.isci.2021.102305

iScience

CellPress
OPEN ACCESS

Article

Semaphorin3E-PlexinD1 signaling in coronary artery and lymphatic vessel development with clinical implications in myocardial recovery

Kazuaki Maruyama,[1,2,11,*] Kazuaki Naemura,[1,3] Yuichiro Arima,[1,4] Yasunobu Uchijima,[1] Hiroaki Nagao,[5] Kenji Yoshihara,[5] Manvendra K. Singh,[6] Akiyoshi Uemura,[7] Fumio Matsuzaki,[8] Yutaka Yoshida,[9] Yukiko Kurihara,[1] Sachiko Miyagawa-Tomita,[1,5,10] and Hiroki Kurihara[1,*]

SUMMARY

Blood and lymphatic vessels surrounding the heart develop through orchestrated processes from cells of different origins. In particular, cells around the outflow tract which constitute a primordial transient vasculature, referred to as aortic subepicardial vessels, are crucial for the establishment of coronary artery stems and cardiac lymphatic vessels. Here, we revealed that the epicardium and pericardium-derived Semaphorin 3E (Sema3E) and its receptor, PlexinD1, play a role in the development of the coronary stem, as well as cardiac lymphatic vessels. *In vitro* analyses demonstrated that Sema3E may demarcate areas to repel PlexinD1-expressing lymphatic endothelial cells, resulting in proper coronary and lymphatic vessel formation. Furthermore, inactivation of Sema3E-PlexinD1 signaling improved the recovery of cardiac function by increasing reactive lymphangiogenesis in an adult mouse model of myocardial infarction. These findings may lead to therapeutic strategies that target Sema3E-PlexinD1 signaling in coronary artery diseases.

INTRODUCTION

The cardiac vascular system is composed of coronary and lymphatic vessel networks. The coronary arteries (CAs) are the first branches of the aorta and supply blood to the heart muscle. During mammalian CA development, endothelial cells derived from a variety of sources, including the proepicardium (Katz et al., 2012; Mikawa and Gourdie, 1996; Pérez-Pomares et al., 2002), endocardium (Wu et al., 2012), and sinus venosus (Red-Horse et al., 2010; Tian et al., 2013b), constitute an initial vascular plexus. Subsequent remodeling leads to maturation of the coronary vasculature and production of proper stems that are connected to the aorta through two ostia originating from the aortic sinuses (Chen et al., 2014a, 2014b). These connections are formed by the process in which endothelial cells from circumferential capillaries surrounding the outflow tract (*i.e.*, the peritruncal vessels) penetrate the aortic wall at the level of the aortic sinuses (Ando et al., 2004; Bogers et al., 1989; Poelmann et al., 1993; Tian et al., 2013a; Waldo et al., 1990). Then, a bilateral pair of ostia is selected from the multiple connections between the peritruncal vessels and the aorta, resulting in the formation of normal left and right CA (Chen et al., 2014a, 2014b). Congenital anomalies that affect the coronary ostia and stems may cause myocardial ischemia and often lead to sudden death (Angelini, 2007; Hauser, 2005). Despite the clinical importance of CA stem formation, the mechanisms underlying this process remain largely unknown.

Recent studies have implicated transient embryonic microvessels surrounding the aorta, termed aortic subepicardial vessels (ASVs), in CA stem formation (Chen et al., 2014a, 2014b). ASVs are thought to be the primary components of peritruncal vessels, later remodeled into CA stems. In contrast, a subset of early ASV endothelial cells express prospero homeobox transcription protein 1 (Prox1), a master regulator of lymphangiogenesis (Chen et al., 2014a, 2014b). ASVs regress at later embryonic stages, whereas lymphatic vessels expressing lymphatic endothelial markers, vascular endothelial growth factor receptor 3 (VEGFR3) and lymphatic vessel endothelial hyaluronic acid receptor 1 (LYVE1), subsequently appear around the aorta (Klotz et al., 2015; Maruyama et al., 2019). However, no detailed analysis has described the possible relationship between ASVs and lymphatic vessels.

[1]Department of Physiological Chemistry and Metabolism, Graduate School of Medicine, The University of Tokyo, 7-3-1 Hongo, Bunkyo-ku, Tokyo 113-0033, Japan

[2]Isotope Science Center, The University of Tokyo, 2-11-16 Yayoi, Bunkyo-ku, Tokyo 113-0032, Japan

[3]Department of Neurosurgery, Graduate School of Medicine, The University of Tokyo, 7-3-1 Hongo, Bunkyo-ku, Tokyo, 113-8655, Japan

[4]Department of Cardiovascular Medicine, Faculty of Life Sciences, Kumamoto University, 2-2-1 Honjo, Kumamoto, Kumamoto 860-0811, Japan

[5]Heart Center, Department of Pediatric Cardiology, Tokyo Women's Medical University, 8-1 Kawada-cho, Shinjuku-ku, Tokyo 162-8666, Japan

[6]Program in Cardiovascular and Metabolic Disorders, Duke-NUS Medical School Singapore, and the National Heart Research Institute Singapore, National Heart Center Singapore, 8 College Road Singapore 169857, Singapore

[7]Department of Retinal Vascular Biology, Nagoya City University Graduate School of Medical Sciences, 1 Kawasumi Mizuho-cho, Mizuho-ku, Nagoya 467-8601, Japan

[8]Laboratory for Cell Asymmetry, RIKEN Center for Developmental Biology, 2-2-3, Minatojiima-Minamimachi, Chuou-ku, Kobe 650-0047, Japan

Continued

Semaphorin 3E (Sema3E) and its receptor PlexinD1 are members of the Sema-Plexin system, originally identified as an axon guidance regulator but currently recognized as a signaling axis regulating diverse (patho)physiological processes, including the morphogenesis and homeostasis of various organs (Corà et al., 2014; Epstein et al., 2015; Kruger et al., 2005; Sandireddy et al., 2019). Although other Sema members, such as Sema3A, 3C, and 4A, interact with PlexinA1 and PlexinD1 via Neuropilin (Nrp)-dependent mechanisms, only Sema3E directly binds to PlexinD1 (Corà et al., 2014; Epstein et al., 2015). Recent evidence has implicated this signaling axis in various vascular processes such as angiogenesis and pathological conditions (Casazza et al., 2010; Fukushima et al., 2011; Moriya et al., 2010; Shimizu et al., 2013). During development, *Sema3e*$^{-/-}$ and *Plxnd1*$^{-/-}$ mutant mice reportedly exhibit aberrant vascularization of the intersomitic vessels (Gu et al., 2005). In particular, *Plxnd1* mutant mice show various cardiovascular anomalies, including high take-off CAs (Gitler et al., 2004; Zhang et al., 2009) and abnormal artery-lymph alignment with reduced lymphatic vessel branching in mouse embryonic back skin (Liu et al., 2016). Although *Sema3c* knockout is reported to cause a laterally dislocated connection to the aortic sinuses (Théveniau-Ruissy et al., 2008), the role of the Sema-Plexin system in coronary and lymphatic vessel formation remains largely unknown.

Here, we revealed a critical role of the Sema3E-PlexinD1 signaling axis in CA stem and cardiac lymphatic vessel development. *Sema3e* and *Plxnd1* mutant mice exhibited excess CA ostia and abnormal cardiac lymphangiogenesis. On investigating the mechanism underlying these anomalies, a close relationship between CA and lymphatic vessel development was observed, suggesting the importance of the Sema3E-PlexinD1 signaling axis in ASV development. In addition, our *in vitro* studies revealed that Sema3E-PlexinD1 signaling was mediated via the actin cytoskeleton and focal adhesion rearrangement to elicit repulsive movement in lymphatic endothelial cells. Furthermore, the inhibition of Sema3E-PlexinD1 signaling significantly improved cardiac function after myocardial injury, possibly by altering the lymphangiogenic response. Our results could provide insights into therapeutic strategies for CA diseases, which remain the leading cause of death in most developed countries.

RESULTS

Sema3e$^{-/-}$ and *Plxnd1*$^{-/-}$ mice exhibit severe CA defects

We performed a phenotypic analysis of *Sema3e*$^{-/-}$ and *Plxnd1*$^{-/-}$ embryos to obtain clues regarding the mechanism underlying CA stem development. As almost all *Plxnd1*$^{-/-}$ mice died by embryonic day 16.5 (E16.5) to E17.0, as previously reported (Zhang et al., 2009), owing to severe systemic edema and hemorrhage, accompanied by systemic vascular malformations (data not shown), we performed immunostaining with the endothelial marker PECAM (platelet endothelial cell adhesion molecule) and confocal imaging on *Sema3e* and *Plxnd1* mutant hearts at E16.5. Although most all of the control hearts exhibited two coronary ostia at the aortic sinuses as expected, the number of coronary ostia was significantly increased in *Sema3e*$^{-/-}$ or *Plxnd1*$^{-/-}$ homozygous hearts (Figures 1A–1D). Occasionally, un-remodeled coronary vessels (CVs) were directly connected to the persistent truncus arteriosus (PTA) wall in *Plxnd1*$^{-/-}$ hearts (Figure 1C). Then, we analyzed postnatal *Sema3e*$^{-/-}$ animals to exclude the possibility that CA phenotypes were induced by a developmental delay. At postnatal day 7 (P7), *Sema3e*$^{-/-}$ hearts still showed an increased number of coronary ostia (Figures 1E and 1F). The supernumerary CA ostia were positioned higher or lower in aortic sinuses but not in the pulmonary artery sinus. Thus, Sema3E-PlexinD1 signaling may control the number of ostia and CA patterns.

Sema3E-PlexinD1 signaling is required for coronary artery remodeling

We performed a sequential analysis of CA development in wild-type mice from E11.5 to E18.5 using PECAM staining to identify the mechanism through which supernumerary CA ostia are formed in mutant mice (Figures S1A and S1B). During normal development, the peritruncal vessels running through the dorsal side of the aorta first emerged at E11.5. These vessels, which were previously described as ASVs (Chen et al., 2014a, 2014b), extended toward the base of the aorta and reached future ostial sites at E12.5, where they communicated with CVs extending from the ventricular wall and connected to the aortic lumen at multiple sites by E13.5. At E15.0, CVs penetrated the aortic sinus at multiple sites in a reticular pattern. At E15.5, the CVs merged to form multiple large mature CAs. These multiple CAs had been remodeled into two mature ostia by E16.5. In *Sema3e*$^{-/-}$ and *Plxnd1*$^{-/-}$ mice, multiple CA ostia had typically formed by E15.5 (Figures 2A and 2B). Thus, the process of CA ostium formation involves penetration of the ASVs into the aortic lumen at E12.5 to E13.5, the connection of the CVs to the aortic sinuses at E13.5 to E15.5, and remodeling into two mature connections at normal ostial sites at E15.5 to E16.5. Sema3E-PlexinD1

[9]Division of Developmental Biology, Cincinnati Children's Hospital Medical Center, Cincinnati, OH 45229, USA

[10]Department of Animal Nursing Science, Yamazaki University of Animal Health Technology, 4-7-2 Minami-Osawa, Hachioji, Tokyo 192-0364, Japan

[11]Lead contact

*Correspondence: k.maruyama0608@gmail.com (K.M.), kuri-tky@umin.net (H.K.)

https://doi.org/10.1016/j.isci.2021.102305

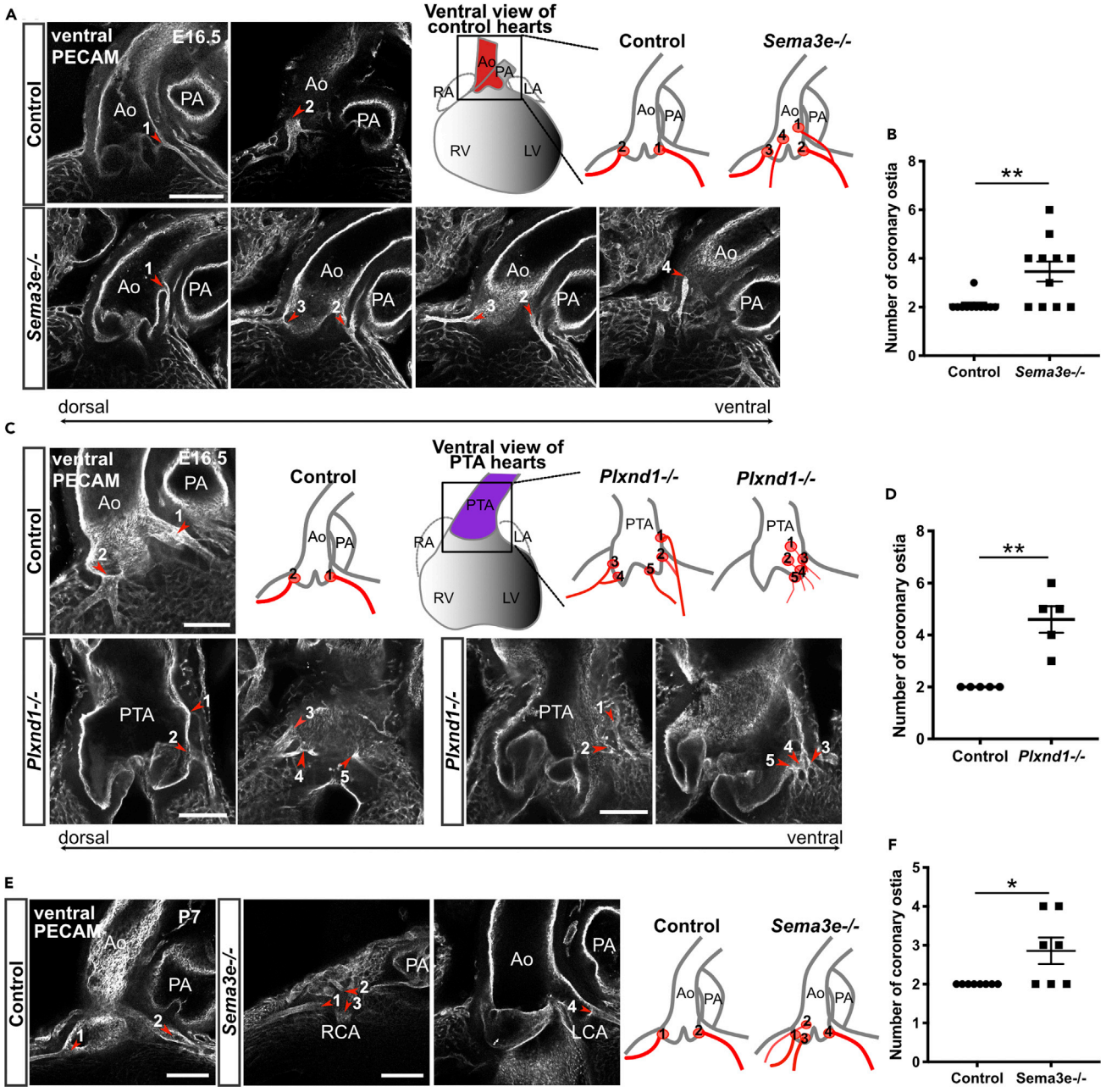

Figure 1. *Sema3e*$^{-/-}$ and *Plxnd1*$^{-/-}$ mice show CA defects

(A, C, and E) Whole-mount confocal images of hearts labeled for PECAM. (A) Images of control and *Sema3e*$^{-/-}$ hearts at E16.5. (C) Images of control and *Plxnd1* $^{-/-}$ hearts at E16.5. *Plxnd1*$^{-/-}$ mice showed PTA. (E) Images of control and *Sema3e*$^{-/-}$ hearts at P7. Control hearts exhibited two ostia at the aortic sinuses (red arrowheads). *Sema3e*$^{-/-}$ and *Plxnd1* $^{-/-}$ hearts showed an increased number of CA ostia and displaced coronary ostia (red arrowheads). Numbers on each schema corresponded to numbers on each figure.

(B, D, and F) Numbers of coronary ostia in control, *Sema3e*$^{-/-}$, and *Plxnd1*$^{-/-}$ hearts were quantified. Ao, aorta; PA, pulmonary artery; PTA, persistent truncus arteriosus; CA, coronary artery. All results are expressed as the means ± standard error of the mean (SEM), and statistical analyses were performed using a non-parametric Mann-Whitney's U test. Each dot represents a value obtained from one sample. *P < 0.05, **P < 0.01. Scale bars, 100 μm (A, C, and E).

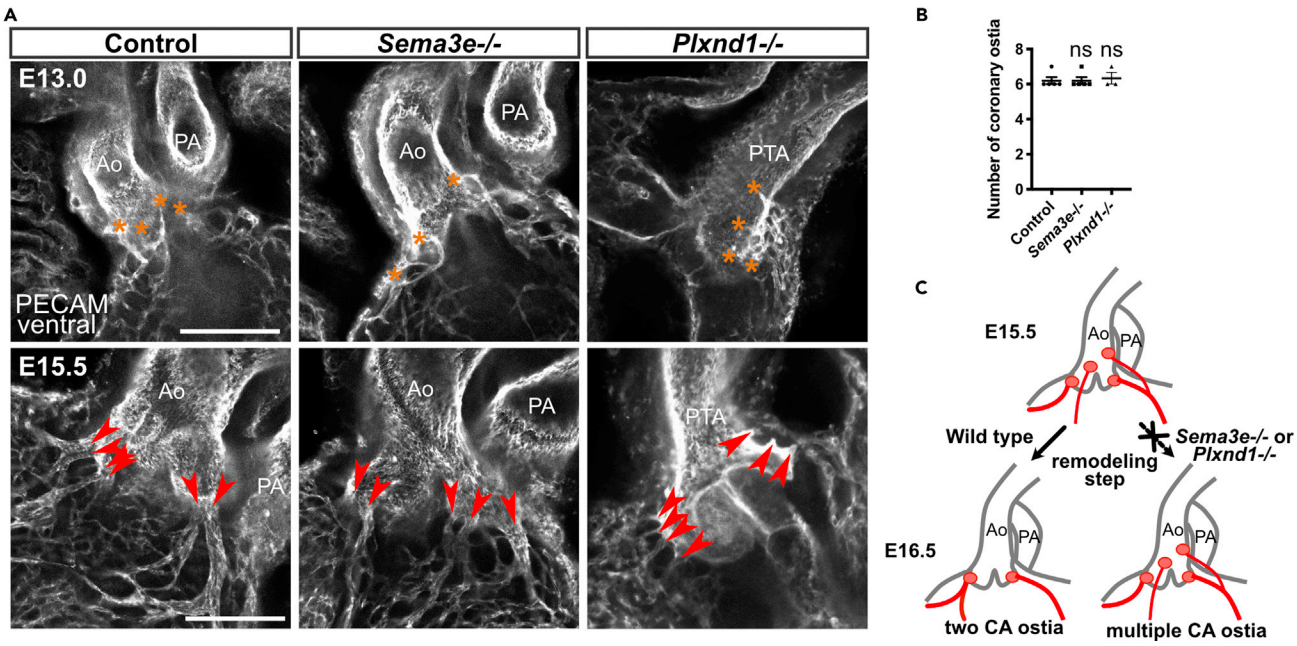

Figure 2. The remodeling step in CA ostium development is disturbed in *Sema3e*$^{-/-}$ and *Plxnd1*$^{-/-}$ mice

(A) Whole-mount confocal images of control, *Sema3e*$^{-/-}$, and *Plxnd1*$^{-/-}$ hearts at E13.0 and E15.5. Orange asterisks represent connections formed between ASVs and the aorta at E13.0. Red arrowheads represent large connections formed between the aorta and CVs at E15.5.

(B) Numbers of coronary ostia in control, *Sema3e*$^{-/-}$, and *Plxnd1*$^{-/-}$ hearts at E15.5 were quantified.

(C) Schematic representation of CA ostium development in control, *Sema3e*$^{-/-}$, and *Plxnd1*$^{-/-}$ mice. Ao, aorta; PA, pulmonary artery; PTA, persistent truncus arteriosus; CV, coronary vessel; CA, coronary artery; ASVs, aortic subepicardial vessels. All results are expressed as the means ± standard error of the mean (SEM), and statistical analyses were performed using a one-way analysis of variance (ANOVA) between groups and post hoc multiple comparisons using Bonferroni's test. Each dot represents a value obtained from one sample. ns, $P \geq 0.05$. Scale bars, 50 μm (A, upper row), 100 μm (A, lower row).

signaling likely contributes to the last step of remodeling to produce two coronary stems at the proper positions (Figure 2C).

Sema3E is expressed in the epicardium, whereas PlexinD1 is expressed in the endothelium

To explore the involvement of Sema3E-PlexinD1 signaling in CA development, we examined Sema3E and PlexinD1 expression patterns in the developing mouse heart through *in situ* hybridization and immunohistochemistry. From the embryonic (E10.5) to postnatal (P7) stages, PlexinD1 was broadly expressed in the endocardium and endothelium of large and small vessels, including CAs (Figure S2A). PlexinD1 was also expressed in lymphatic endothelial cells (LECs) at E16.5 (Figure S2C). These PlexinD1 signals were abolished in *Plxnd1*$^{-/-}$ hearts at E16.5, confirming their specificity in blood and lymphatic endothelial cells (Figures S2B and S2C). Subsequently, we analyzed *Sema3e* expression using *in situ* hybridization. *Sema3e* was expressed in the bronchial and esophageal epithelium, as well as somites at E11.5, E13.5, and E15.5 (Figures 3A, 3E, and 3I). In the heart, *Sema3e* was expressed in the mesenchyme at the base of the outflow tract, the pericardium, and the epicardium at E11.5 (Figures 3A–3D). Although mesenchymal expression was not observed at E13.5 and E15.5, pericardial and epicardial expressions were well maintained (Figures 3E–3L). At E13.5 and E15.5, a stronger expression was observed in the aortic epicardium and sinus venosus (Figures 3F, 3H, 3J, and 3L). These *Sema3e* signals were abolished in the *Sema3e*$^{-/-}$ hearts at E14.5, confirming their specificity (Figures 3M–3P).

Disruption of Sema3E-PlexinD1 signaling leads to cardiac lymphatic vessel malformation

Next, we examined whether lymphatic vessel development was affected in mice lacking Sema3E-PlexinD1 signaling by employing vascular and lymphatic endothelial markers. We first tested PECAM, Prox1, and VEGFR3 expression patterns. Consistent with our previous work (Maruyama et al., 2019), PECAM^{+}/Prox1^{+}/VEGFR3^{+} lymphatic vessels were distributed around the aorta and dorsal side of ventricles in control and *Sema3e*$^{-/-}$ embryos at E16.5 (Figures 4A and 4B). In *Sema3e*$^{-/-}$ embryos, lymphatic vessels were

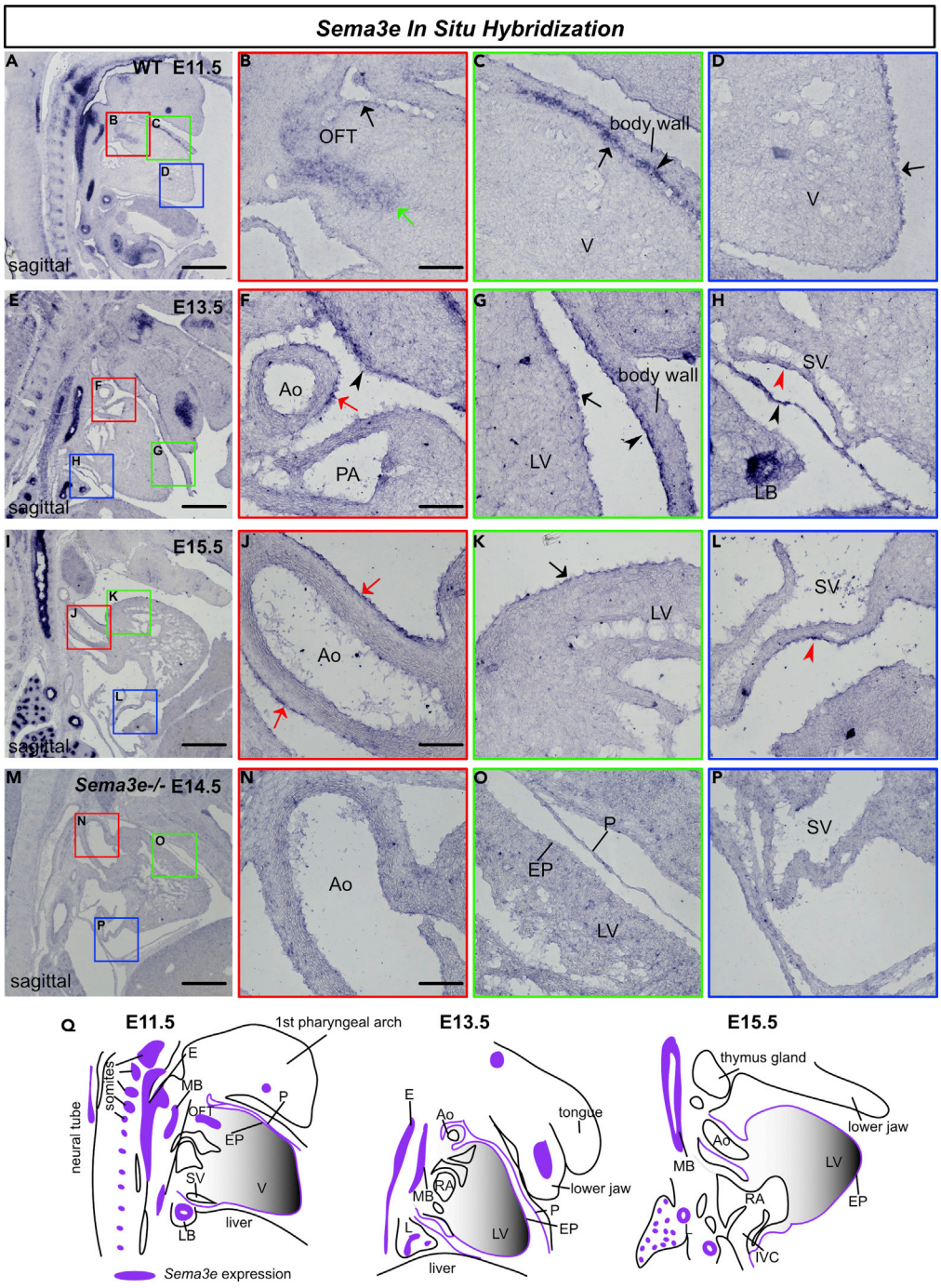

Figure 3. *Sema3e* is expressed in the developing heart

(A–P) Sagittal section *in situ* hybridization for *Sema3e* mRNA. (A–L) At E11.5, E13.5, and E15.5, *Sema3e* was expressed in the somites, nerves, and esophageal and bronchial epithelium. In the heart, *Sema3e* was expressed in the pericardium (black arrow heads), epicardium (black arrows), aortic epicardium (red arrows), and sinus venosus (red arrowheads). At E11.5, *Sema3e* was expressed at the base of the outflow tracts (green arrow). (M–P) *Sema3e* expression was absent in *Sema3e*$^{-/-}$ embryos at E14.5.

(Q) Schematic view of *Sema3e* expression. The boxed areas are magnified in the right images. OFT, outflow tract; V, ventricle; Ao, aorta; PA, pulmonary artery; LV, left ventricle; LB, lung bud; SV, sinus venosus; EP, epicardium; P, pericardium; E, esophagus; MB, main bronchus; L, lung; RA, right atrium; IVC, inferior vena cava. Scale bars, 500 μm (A, E, I, M), 100 μm (B, F, J, N)

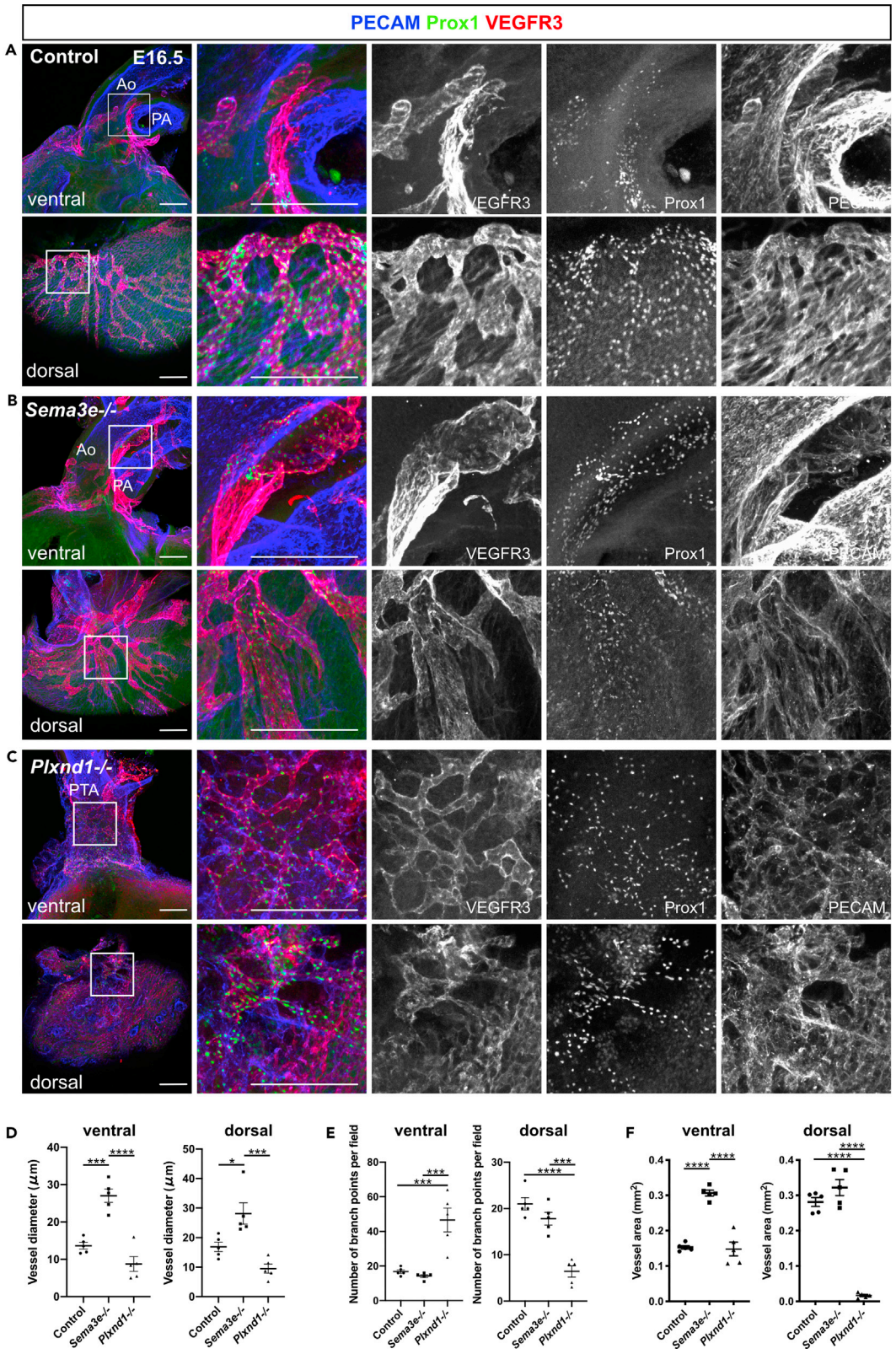
PECAM Prox1 VEGFR3
A
Control E16.5
Ao
PA
ventral
dorsal
VEGFR3
Prox1
B
Sema3e-/-
C
Plxnd1-/-
PTA
PECAM
D
ventral
dorsal
Vessel diameter (μm)
Control
Sema3e-/-
Plxnd1-/-
E
Number of branch points per field
F
Vessel area (mm²)

Figure 4. Sema3E-PlexinD1 signaling contributes to cardiac lymphatic vessel development

(A–C) Whole-mount confocal images of control, *Sema3e*$^{-/-}$, or *Plxnd1*$^{-/-}$ hearts labeled for PECAM, Prox1, and VEGFR3.

(D–F) Quantification of vessel diameter (D), number of branch points (E), and vessel area of ventral and dorsal side of the ventricles (F) (five points were counted in each sample). VEGFR3^{+} vessel areas were calculated using AngioTool. Ao, aorta; PA, pulmonary artery; PTA, persistent truncus arteriosus. All results are expressed as the means ± standard error of the mean (SEM), and statistical analyses were performed using a one-way analysis of variance (ANOVA) between groups and post hoc multiple comparisons using Bonferroni's test. Each dot represents a value obtained from one sample. *P < 0.05, ***P < 0.001, ****P < 0.0001. Scale bars, 100 μm (A-C).

dilated and hyperplastic when compared with control vessels (Figures 4A, 4B, 4D, and 4F). Conversely, *Plxnd1*$^{-/-}$ embryos showed a fine plexus of lymphatic vessels with increased branch points surrounding the PTA wall (Figures 4C–4F). On the dorsal side of ventricles, *Plxnd1*$^{-/-}$ embryos also exhibited fine lymphatic vessels without large remodeled lymphatic vessels (Figures 4C, 4D, and 4F). We further tested LYVE1 expression patterns in control, *Sema3e*$^{-/-}$ and *Plxnd1*$^{-/-}$ embryos. Consistent with VEGFR3 expression patterns, in *Sema3e*$^{-/-}$ hearts, LYVE1^{+} lymphatic vessels were abnormally thickened when compared with control hearts (Figures 5A and 5B). By contrast, LYVE1^{+} areas were relatively sparse and discontinued without forming a reticulated structure around the PTA wall of *Plxnd1*$^{-/-}$ embryos (Figure 5C). In addition, only a small part of PECAM^{+}/Prox1^{+} cells expressed LYVE1 (Figure 5C). Consistently, the vessel area of LYVE1^{+} lymphatic vessels was increased in *Sema3e*$^{-/-}$ embryos at E16.5, whereas mature lymphatic vessel formation appeared defective in *Plxnd1*$^{-/-}$ embryos (Figures 5D and 5E). These phenotypes were also observed in the dorsal ventricular wall (Figures S3A–S3C).

To compare peripheral and cardiac lymphatic vessel development, we analyzed lymphatic vessel development in *Sema3e*$^{-/-}$ and *Plxnd1*$^{-/-}$ embryos using dorsal skin. In *Sema3e*$^{-/-}$ and *Plxnd1*$^{-/-}$ embryos, the distance between from each migration front to the midline was shorter than control (Figures S4A and S4C). *Sema3e*$^{-/-}$ and *Plxnd1*$^{-/-}$ embryos displayed dilated lymphatic vessels and reduced lymphatic vessel branching (Figures S4A, S4D, and S4E), as previously reported (Liu et al., 2016). Excessive sprouts were observed in *Sema3e*$^{-/-}$ and *Plxnd1*$^{-/-}$ embryos (Figures S4B and S4F). These results indicate the importance of Sema3E and PlexinD1 in cardiac and peripheral lymphatic vessel development; however, these appear to exert opposite effects in the heart. The phenotypic discrepancy between *Sema3e*$^{-/-}$ and *Plxnd1*$^{-/-}$ mice may be attributed to other semaphorin members, such as Sema3A and Sema3C (see the Discussion).

Sema3E-PlexinD1 signaling induces the repulsion and cytoskeletal collapse of LECs

Reportedly, Sema3E-PlexinD1 signaling negatively regulates angiogenesis in blood endothelial cells by inhibiting VEGF-A-VEGFR2 downstream signaling (Fukushima et al., 2011; Moriya et al., 2010). However, there have been no reports on the effect of Sema3E-PlexinD1 signaling on LECs. To investigate the molecular mechanism underlying the observed biological effects of Sema3E-PlexinD1 signaling on LECs, we performed *in vitro* studies using cultured human primary LECs (HLECs). To investigate the effect of Sema3E-PlexinD1 signaling on cell motility, we first performed scratch-wound-healing assays using recombinant Sema3E protein. Compared with control cells, wound healing was significantly impaired in Sema3E-treated HLECs (Figures S5A and S5B). Wound healing involves both migration and proliferation; accordingly, we analyzed the effect of Sema3E on cell proliferation using the MTT assay. Sema3E inhibited the proliferation of HLECs (Figure S5C), suggesting that decreased proliferation may partly explain the Sema3E-induced impairment of wound healing. In LECs, VEGFR3 activation by VEGF-C induces proliferation, migration, and survival, partly through extracellular signal-regulated kinase 1/2 (ERK1/2) and AKT phosphorylation (Adams and Alitalo, 2007). However, Sema3E stimulation did not affect VEGF-C-induced phosphorylation of ERK1/2 and AKT (Figure S5D). We further analyzed the effect of Sema3E on HLEC motility using HEK-293T cells expressing Sema3E. When Sema3E-expressing HEK-293T cells were seeded onto subconfluent HLECs, they repelled HLECs, whereas HEK-293T cells containing empty expression vector did not (Figures 6A–6C) (referred to as LEC repulsive assay). We also verified that Sema3E specifically acted through PlexinD1 in HLECs by using small interfering RNA (siRNA). First, we tested the efficiency of siRNA by western blotting against PlexinD1 and confirmed the downregulation of PlexinD1 protein levels (Figures S5E and S5F). When Sema3E-expressing HEK-293T cells were seeded onto subconfluent siControl transfected HLECs, they repelled HLECs, whereas control HEK-293T cells containing empty expression vector did not demonstrate similar behavior (Figures 6D–6F). These repulsive activities were nullified by siPlexinD1 (Figures 6E and 6F).

To mimic the *in vivo* repulsive activity of Sema3E-PlexinD1 signaling against lymphatic vessel growth and patterning, we employed aggregates of HLECs (LEC spheroid sprouting assay) with control- or

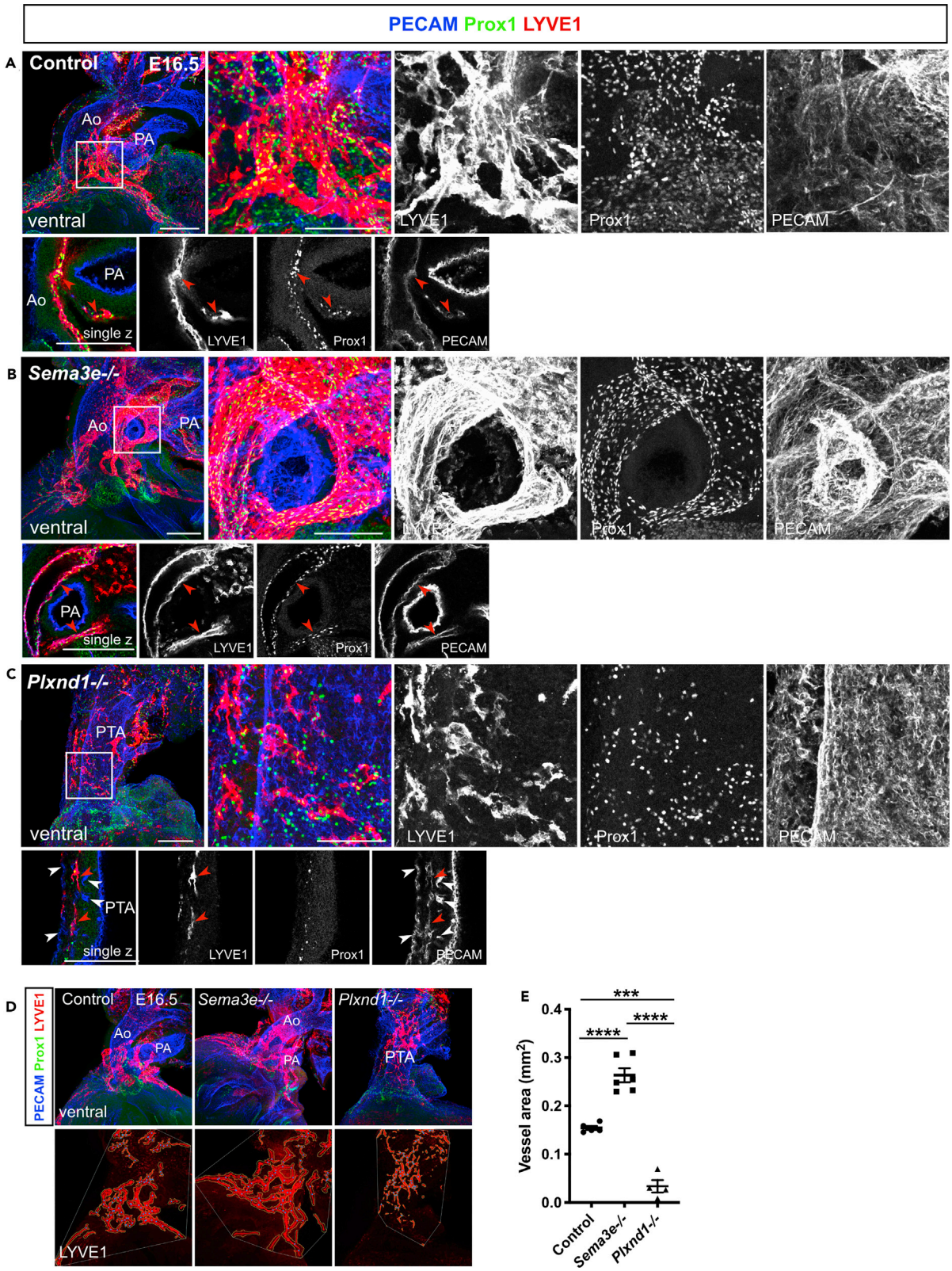
PECAM Prox1 LYVE1
A
Control
E16.5
Ao
PA
ventral
LYVE1
Prox1
PECAM
PA
Ao
single z
LYVE1
Prox1
PECAM
B
Sema3e-/-
Ao
PA
ventral
LYVE1
Prox1
PECAM
PA
single z
LYVE1
Prox1
PECAM
C
Plxnd1-/-
PTA
ventral
LYVE1
Prox1
PECAM
PTA
single z
LYVE1
Prox1
PECAM
D
PECAM Prox1 LYVE1
Control
E16.5
Sema3e-/-
Plxnd1-/-
Ao
PA
PTA
ventral
LYVE1
E
Vessel area (mm2)
0.4
0.3
0.2
0.1
0.0
***
****
****
Control
Sema3e-/-
Plxnd1-/-

Figure 5. LYVE1 expression patterns in control, *Sema3e*$^{-/-}$, and *Plxnd1*$^{-/-}$ hearts

(A–C) Whole-mount confocal images of control, *Sema3e*$^{-/-}$, or *Plxnd1*$^{-/-}$ hearts labeled for PECAM, Prox1, and LYVE1 at E16.5. (A and B) In control and *Sema3e*$^{-/-}$ hearts, PECAM, Prox1, and LYVE1 were co-expressed in lymphatic vessels (red arrow heads). (C) In *Plxnd1*$^{-/-}$ hearts, hyperplastic PECAM^{+} capillaries were recognized in the PTA wall (white arrowheads). Fewer PECAM^{+}/Prox1^{+}/LYVE1^{+} lymphatic vessels (red arrowheads) were observed on the PTA wall.

(D) Confocal images of control, *Sema3e*$^{-/-}$, or *Plxnd1*$^{-/-}$ hearts at E16.5 captured for AngioTool analyses. The LYVE1^{+} vessels (red) and branch points (blue) were depicted, which enabled the quantitative assessment of vessel parameters.

(E) Quantification of the LYVE1^{+} vessel area. Ao, aorta; PA, pulmonary artery; PTA, persistent truncus arteriosus. All results are expressed as the means ± standard error of the mean (SEM), and statistical analyses were performed using a one-way analysis of variance (ANOVA) between groups and post hoc multiple comparisons using Bonferroni's test. Each dot represents a value obtained from one sample. ***P < 0.001, ****P < 0.0001. Scale bars, 100 μm (A-C)

Sema3E-expressing HEK-293T cells (Figures 6G–6J). We first attempted to establish aggregates with si-PlexinD1 transfected HLECs; however, we were unable to obtain proper spheroids to evaluate the repulsive activity of Sema3E-PlexinD1 as both the number and branch length of sprouting were dramatically decreased when compared with controls (data not shown). Thus, we used untreated HLECs to form spheroids. In spheroids co-cultured with Sema3E-expressing HEK-293T cells, branch elongation was hindered in the vicinity of Sema3E-expressing cells, as reflected by a significant decrease in the number and length of sprouts in the direction of GFP^{+} (Sema3E-expressing) cells compared to the opposite direction (Figures 6H–6J), leading to cell-free area formation.

Live imaging revealed that Sema3E-expressing cells caused a remarkable change in the shape of HLECs, rapidly repelling HLECs (Figure S6A and Video S1). A compilation of the tracks corresponding to individual HLEC migration paths showed that Sema3E-expressing HEK-293T cells repelled HLECs, which migrated with significantly increased velocity when compared with cells far from Sema3E-expressing cells (Figures S6B, S6C, and Video S2). Moreover, the velocity appeared to correlate with the distance from Sema3E-expressing cells (Figure S6D). Notably, HLECs avoided areas where Sema3E-expressing cells passed, even though they did not contact each other directly. Considering that Sema3E is a secreted protein, it may demarcate areas that repel the formation of lymphatic vessels in a dose-dependent manner.

Semaphorins were characterized in part based on their ability to drastically alter actin cytoskeletal dynamics in neuronal and vascular processes (Hamm et al., 2016; Hung et al., 2010). Furthermore, recent evidence has shown that Sema3E signaling through PlxnD1 regulates vascular patterning by modulating the cytoskeleton and focal adhesion structures (Aghajanian et al., 2014; Sakurai et al., 2010). To elucidate the effect of Sema3E-PlexinD1 signaling on morphological changes in HLECs, we evaluated evoked cytoskeletal remodeling and focal adhesion in HLECs by staining actin fibers with fluorescence-labeled phalloidin and focal adhesion plaques with immunostaining for vinculin. Sema3E treatment inhibited actin stress fiber formation and induced contraction in HLECs when compared with the control (Figure S5G). The cell percentage demonstrating a loss of dense stress fibers increased significantly in the Sema3E-treated groups when compared with the control (Figure S5H). Concurrently, focal adhesion plaques visualized by vinculin staining also decreased in number following Sema3E exposure (Figures S5G and S5I). The loss of actin stress fibers and focal adhesion plaques after Sema3E treatment was abolished by siPlexinD1 (Figures S5J–S5L), indicating that Sema3E specifically acted through PlexinD1 to induce detachment and collapses of the actin cytoskeleton, resulting in increased cell motility.

Collectively, these results suggest that Sema3E, acting through PlexinD1, suppressed HLEC proliferation and repelled them by demarking HLEC-free areas, possibly by regulating the actin cytoskeleton and focal adhesion, which may contribute to proper positioning of lymphatic vessels.

Inhibition of Sema3E improves cardiac function and alters lymphatic phenotypes following cardiac injury

Lymphangiogenesis has recently been implicated in post-cardiac injury syndrome. The stimulation of lymphangiogenesis by VEGF-C improves cardiac function after myocardial infarction (MI) (Henri et al., 2016; Klotz et al., 2015). *Sema3e*$^{-/-}$ mice presented hyperplastic cardiac lymphatic vessels (Figures 4 and 5). Additionally, our *in vitro* studies indicated that Sema3E-PlexinD1 signaling affected lymphatic endothelial cell migration and proliferation (Figures 6, S5 and S6). Therefore, we hypothesized that the inhibition of Sema3E-PlexinD1 signaling might improve cardiac function after MI via a lymphangiogenic mechanism. First, we evaluated the protein levels of Sema3E and VEGFR3 in the infarcted area of the left ventricle. Sema3E protein levels increased rapidly one week post-MI. VEGFR3 protein levels also increased following infarction (Figure 7A). Sema3E was produced

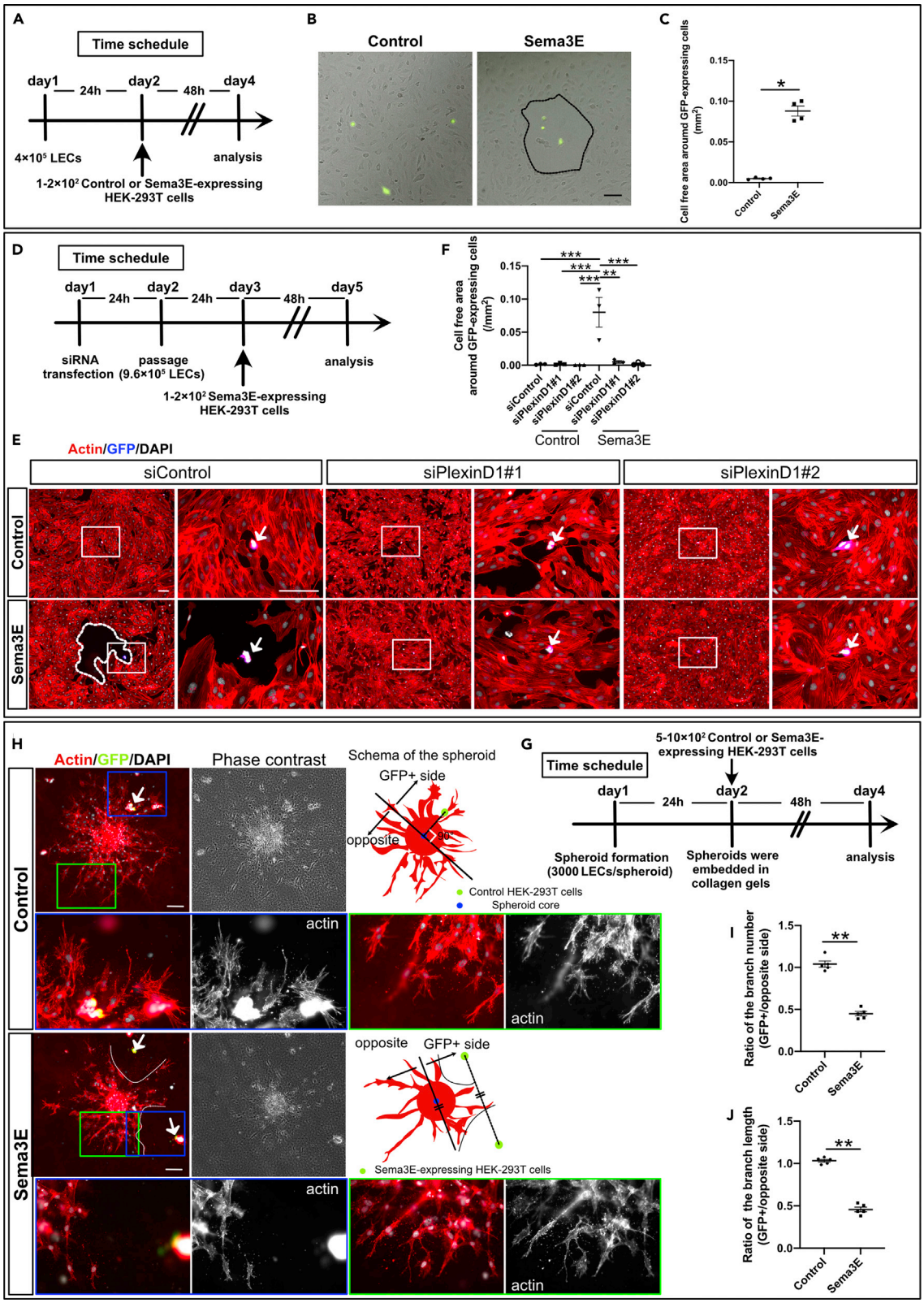
A
Time schedule
day1
24h
day2
48h
day4
4×10⁵ LECs
analysis
1-2×10² Control or Sema3E-expressing HEK-293T cells
B
Control
Sema3E
C
Cell free area aroumd GFP-expressing cells (mm²)
0.15
0.10
0.05
0.00
*
Control
Sema3E
D
Time schedule
day1
24h
day2
24h
day3
48h
day5
siRNA transfection
passage (9.6×10⁵ LECs)
analysis
1-2×10² Sema3E-expressing HEK-293T cells
F
Cell free area aroumd GFP-expressing cells (/mm²)
0.15
0.10
0.05
0.00
***
***
***
***
**
siControl
siPlexinD1#1
siPlexinD1#2
siControl
siPlexinD1#1
siPlexinD1#2
Control
Sema3E
E
Actin/GFP/DAPI
siControl
siPlexinD1#1
siPlexinD1#2
Control
Sema3E
H
Actin/GFP/DAPI
Phase contrast
Schema of the spheroid
GFP+ side
opposite
90°
Control HEK-293T cells
Spheroid core
actin
opposite
GFP+ side
Sema3E-expressing HEK-293T cells
G
Time schedule
5-10×10² Control or Sema3E-expressing HEK-293T cells
day1
24h
day2
48h
day4
Spheroid formation (3000 LECs/spheroid)
Spheroids were embedded in collagen gels
analysis
I
Ratio of the branch number (GFP+/opposite side)
1.5
1.0
0.5
0.0
**
Control
Sema3E
J
Ratio of the branch length (GFP+/opposite side)
1.5
1.0
0.5
0.0
**
Control
Sema3E

Figure 6. Sema3E-expressing cells repel lymphatic endothelial cells

(A) Time schedule for the LEC repulsive assays.

(B and C) (B) Control HEK-293T cells transfected with pFLAG-T2A-EGFP vectors (control) or HEK-293T cells transfected with pFLAG-Sema3E-T2A-EGFP (Sema3E) were seeded on top of HLECs. Shown are merged phase-contrast and fluorescence images taken after 48 hr. Cell-free area is marked with a dotted black line and quantified in (C) (n = 4, biological replicates in all conditions. Three areas were counted in each condition).

(D) Time schedule for the siRNA transfected LEC repulsive assays.

(E and F) (E) HLECs were transfected with control siRNA or siPlexinD1. Control HEK-293T cells transfected with pFLAG-T2A-EGFP vectors (control) or HEK-293T cells transfected with pFLAG-Sema3E-T2A-EGFP (Sema3E) were seeded on top of siRNA transfected HLECs. Cell-free area is marked with a dotted white line and the boxed area is magnified in the right box. Cell-free area was quantified in (F) (n = 3, biological replicates in all conditions. Three areas were counted in each condition).

(G) Time schedule for the LEC spheroid sprouting assay.

(H) Spheroids and control or Sema3E-expressing HEK-293T cells were embedded in type I collagen gel and incubated in EGM2 medium. After 48 hr, spheroids and HEK-293T cells were stained for F-actin, GFP, and DAPI. The blue box represented spheroid branches facing to the GFP-expressing HEK-293T cell, and the green box represented control branches. Boxed area was magnified in lower boxes.

(I and J) Spheroids surrounded by 1 or 2 GFP-expressing cells were subjected to quantification. For analyzing the branch number and branch length, spheroids were divided into two parts (GFP^+ cells containing side and the opposite side), depicted in the schema. For statistical analysis, spheroids located near a single GFP-expressing cell were divided by a line orthogonally crossed with a straight line traveling a GFP-expressing cell and the spheroid core. Spheroids surrounded by two GFP-expressing cells were divided by a line through the spheroid core parallel to a line connecting the two GFP-expressing cells. (n = 5, biological replicates in all conditions. Four spheroids were quantified in each condition). All results are expressed as the means ± standard error of the mean (SEM), and statistical analyses were performed using a one-way analysis of variance (ANOVA) between groups, post hoc multiple comparisons, Bonferroni's test (F), or non-parametric Mann-Whitney's U test (C, I, J). $^{**}P < 0.01$, $^{*}P < 0.05$. Scale bar, 100 μm (B, E, H)

in the intact myocardium of the infarcted area (Figure 7B). In contrast, PlexinD1 was produced in the $LYVE1^+$/$VEGFR3^+$ lymphatic vessels and capillaries positive for endomucin (EMCN), a marker of endothelial cells, in and/or around the infarcted area (Figure 7C). We performed immunohistochemistry for PECAM and LYVE1 to observe phenotypic changes in the vasculature of MI hearts. On day 28 post-MI, we identified the presence of a boundary between infarcted and non-infarcted areas (Figures S7A and S7C). LYVE1 signals were also colocalized with Iba1, a marker for macrophages and microglia, indicating macrophage infiltration (Figure S7B). In non-infarcted areas, dense capillaries and CVs were observed in regular patterns, along with reactive $LYVE1^+$ lymphangiogenesis (Figure S7C). In infarcted areas, curved, distended abnormal vessels and a few thin $LYVE1^+$ lymphatic vessels were present (Figure S7D). We then injected Phosphate-buffered saline (PBS) or the recombinant human PlexinD1 protein on days 0, 2, 3, 4, and 6 post-MI to inhibit Sema3E signaling. The use of human PlexinD1 protein to antagonize the effect of mouse Sema3E has been validated in previous studies (Casazza et al., 2010; Tata et al., 2014); additionally, we confirmed the inhibitory effect of human PlexinD1 protein against Sema3E using the LEC repulsive assay (Figures S8A and S8B). On day 28 post-MI, stronger lymphangiogenic responses were observed in regions surrounding injured areas in PlexinD1-treated mice when compared with control mice (Figures 7D and S8C). Distended lymphatic vessels were well developed and covered infarcted areas in PlexinD1-treated mice. Conversely, the newly formed lymphatic vasculature in PBS-treated mice covered relatively smaller areas (Figure S8C). We statistically analyzed EMCN, LYVE1, and VEGFR3 staining in vessels in the infarcted area. The number of $EMCN^+$ and $LYVE1^+$ vessels was significantly increased in PlexinD1-treated mice (Figure 7E). We further analyzed the lymphatic phenotypes on day 28 post-MI. PlexinD1-treated mice demonstrated a significant increase in the number of large $LYVE1^+$ and $VEGFR3^+$ vessels (Figure 7E). Notably, PlexinD1-treated mice exhibited significant improvements in cardiac function, as evidenced by the decreased left ventricular dimensions in diastole and systole (Figure 7F), accompanied by an increased ejection fraction and fractional shortening (Figure 7G). Significantly smaller fibrotic areas and left ventricle wall thinning were observed in PlexinD1-treated mice on day 28 post-MI when compared with controls (Figures 7H and S8E). Furthermore, Sema3E-PlexinD1 signaling is important for immunomodulation and neuronal development. To determine whether recombinant PlexinD1 affected the immune response, we evaluated the number of macrophages in the infarcted area with macrophage marker Iba1. However, we observed no difference in the number of $Ib11^+$ macrophages (Figures S8F–S8H). We evaluated cardiac innervation in the infarcted area using the neuronal marker Tuj1 antibody. However, we failed to observe any difference in the number of $Tuj1^+$ neurons (data not shown). In summary, the inhibition of Sema3E signaling in MI hearts increased the number of capillaries and large lymphatic vessels when compared with control mice, thus improving cardiac function.

DISCUSSION

The present study reveals a role for Sema3E-PlexinD1 signaling in CA stem development that involves remodeling to produce the two coronary ostia at proper positions in the aortic sinuses. Sema3E-PlexinD1 signaling is essential for the proper formation of cardiac lymphatic vessels. This study further revealed

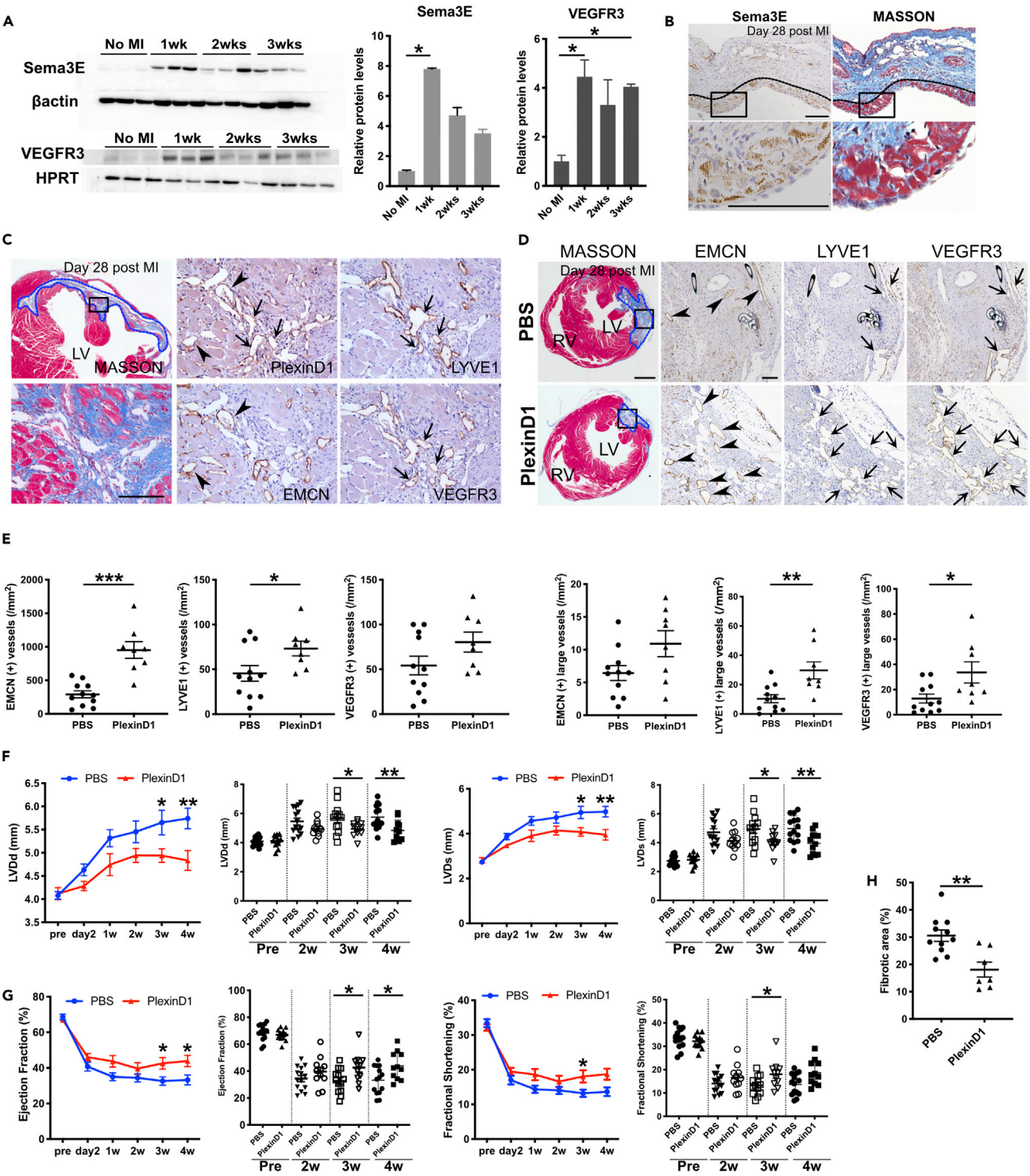

Figure 7. Inhibition of Sema3E-PlexinD1 signaling stimulates lymphangiogenesis and improves cardiac function after myocardial infarction

(A) Western blot analysis of Sema3E and VEGFR3 expression levels. Samples were collected from injured left ventricles of MI hearts (n = 3 animals analyzed per time point and n = 3, biological replicates in all conditions).

(B–D) Serial sections of 4-μm of MI hearts were labeled for Sema3E, PlexinD1, EMCN, LYVE1, VEGFR3, or Masson's trichrome solution. (B) Images of immunolabeling for Sema3E and Masson's trichrome staining in MI hearts. Sema3E could be observed in the intact myocardium of the infarcted area (black dotted lines). Boxed areas are magnified in the lower images. (C) Images of Masson's trichrome staining and immunostaining for EMCN, LYVE1, VEGFR3, and PlexinD1. PlexinD1 was expressed in EMCN^{+} capillaries (black arrowheads) and LYVE1^{+}/VEGFR3^{+} lymphatic vessels in the infarcted area (black arrows).

Figure 7. *Continued*

(D) Paraffin section images of PBS- and recombinant PlexinD1-treated (PlexinD1) MI hearts labeled for Masson's trichrome staining and EMCN, LYVE1, and VEGFR3. Infarcted areas are magnified in the right images. Blue dotted areas represent infarcted regions (C, D).

(E) The numbers of EMCN, LYVE1, and VEGFR3$^+$ vessels in the infarcted area were quantified. Large vessels were defined as vessels with an area >0.003 mm^2. n = 11 (PBS) and n = 8 (PlexinD1).

(F) Evaluation of LV cavity dimensions in end-diastole and end-systole of PBS- or recombinant PlexinD1-treated (PlexinD1) MI mice by echocardiography at the indicated times.

(G) Evaluation of the ejection fraction (EF) and fractional shortening (FS) of PBS- or recombinant PlexinD1-treated (PlexinD1) MI mice by echocardiography at the indicated times.

(H) Evaluation of the fibrotic area of PBS- or recombinant PlexinD1-treated mice (PlexinD1) at day 28 post-MI. LV, left ventricle; RV, right ventricle; MI, myocardial infarction. All results are expressed as the means ± standard error of the mean (SEM), and statistical analyses were performed using a one-way analysis of variance (ANOVA) between groups and post hoc multiple comparisons using Bonferroni's test (A) or non-parametric Mann-Whitney's U test (E, F, G, H). Each dot represents a value obtained from one sample. *P < 0.05, **P < 0.01, ***P < 0.001. Scale bars, 100 μm (B, C, and D, right side images), 500 μm (D, left side image).

the beneficial effect of Sema3E-PlexinD1 signal inhibition on post-MI cardiac dysfunction in adult mice by modulating angiogenic and lymphangiogenic activities in injured hearts.

CA stems were recently reported to be patterned in two steps: the establishment of peritruncal vessels, which are composed of ASVs and immature CVs derived from the proepicardium (Katz et al., 2012; Mikawa and Gourdie, 1996; Pérez-Pomares et al., 2002), endocardium (Wu et al., 2012), and sinus venosus (Chen et al., 2014a, 2014b; Red-Horse et al., 2010). These peritruncal vessels were remodeled and interconnected with the aortic endothelium (Chen et al., 2014a, 2014b; Ivins et al., 2015; Théveniau-Ruissy et al., 2016). The first step requires several molecules including VEGF-C (Chen et al., 2014a, 2014b), C-X-C motif chemokine ligand 12 (Ivins et al., 2015), and the collagen- and calcium-binding EGF-like domains 1 protein (Bonet et al., 2018). Deletion of these signals results in a lack of ASVs and hypoplastic peritruncal CVs, leading to a decrease in the number of CA stems (Chen et al., 2014a, 2014b; Ivins et al., 2015; Théveniau-Ruissy et al., 2016). Cardiomyocytes along the wall of the aorta contribute to the next step by guiding CA stem formation to aortic sinuses (Chen et al., 2014a, 2014b; Théveniau-Ruissy et al., 2016). In the present study, subsequent remodeling of multiple connections into the two CA stems requires Sema3E-PlexinD1 signaling, and the absence of this signaling induces the formation of excess CA ostia positioned randomly at the aortic root.

Our previous report shows that Prox1$^+$/VEGFR3$^+$ mesh-like structures appear around the outflow tract of embryonic mouse hearts around E12.5. These structures are remodeled into Prox1$^+$/VEGFR3$^+$ thickened lymphatic vessels around E15.0 to E16.5 and thereafter extend to the ventral side of the heart. LYVE1 expression in cardiac lymphatic vessels is also recognized at this stage (Maruyama et al., 2019). Conversely, ASVs appeared on the outflow tract around E11.5 and then expanded. These vessels form channels to the aortic lumen and contain blood cells, indicating them to be blood vessels; however, a subset of early ASV endothelial cells is reported to express Prox1 (Chen et al., 2014a, 2014b). Thus, the Prox1$^+$ and/or VEGFR3$^+$ mesh-like structures on the outflow tract wall described in our previous work seem to overlap with ASVs. Taken together with these findings, ASVs and cardiac lymphatic vessels may share a common Prox1$^+$ cell origin. Furthermore, our recent report also shows that some cardiac lymphatic vessels are derived from the Isl1-expressing pharyngeal mesoderm (Maruyama et al., 2019). Moreover, Théveniau-Ruissy et al., using genetic lineage tracing with Cx40-CreERT2 and avian homo-transplantation, have reported that endothelial cells of the CA stem may have different origins from ventricular CAs. They are likely to arise from mesenchyme distal to the outflow tract (Théveniau-Ruissy et al., 2016). These results suggest that ASVs may appear as a primitive mesenchymal plexus which gives rise to blood vessels including CA stems and lymphatic vessels surrounding the outflow tract. During these developmental processes, Sema3E-PlexinD1 signaling may contribute to CA stem remodeling and normal lymphatic development.

Both *Sema3e*$^{-/-}$ and *Plxnd1*$^{-/-}$ mice exhibit excess CA stem formation, but the phenotype related to lymphatic vessel formation is different. In the heart, *Sema3e*$^{-/-}$ mice showed distended lymphatic vessels, whereas *Plxnd1*$^{-/-}$ mice exhibited fine lymphatic plexus positive for VEGFR3 with aberrant LYVE1 expression. In the dorsal skin, both *Sema3e*$^{-/-}$ and *Plxnd1*$^{-/-}$ mice showed an increased lymphatic vessel diameter and reduced branch numbers. This dissimilarity may be attributed to the involvement of the possible Sema3E antagonism to other semaphorin ligands or co-receptors, such as Sema3A, Sema3C, Sema4A, or Nrp1/2, which may stimulate lymphatic vessel formation upon PlexinD1 activation. In fact, Sema-Plexin signaling shows various redundancies (Gu et al., 2003; Toyofuku et al., 2008). *Sema3a*$^{-/-}$ mice present right-sided cardiac hypertrophy, sinus bradycardia owing to defective sympathetic patterning and lymphatic valve defects (Behar et al., 1996; Bouvrée et al., 2012; Ieda et al., 2007). *Sema3c*$^{-/-}$ mice exhibit

PTA and an interrupted aortic arch (Feiner et al., 2001). Sema4A has also been shown to interact with PlexinD1 via Nrp-dependent mechanisms, but Sema4A deletion in mice does not lead to cardiovascular phenotypes (Toyofuku et al., 2007). These findings indicate that PlexinD1 is involved in different aspects of cardiovascular development with various ligand requirements. Additionally, a recent finding suggests a possible role for PlexinD1, forming a complex with VEGFR2 and Nrp1, as a shear stress mechanoreceptor without ligand requirements (Mehta et al., 2020). Thus, the phenotypic discrepancy in cardiac lymphatic vessel formation in *Sema3e*$^{-/-}$ and *Plxnd1*$^{-/-}$ mice may be attributed to redundancy among other semaphorin ligands in the PlexinD1-mediated stimulation or ligand-independent PlexinD1 signaling.

Our *in vitro* studies in HLECs suggest that Sema3E acts on PlexinD1 to induce actin filament reorganization and focal adhesion disassembly, leading to retraction and repulsion of HLECs. Remarkably, Sema3E secreted from transfected HEK-293T cells demarcated areas that repel HLECs through PlexinD1. This, in turn, may contribute to the ability of Sema3E to block HLEC proliferation and migration, thereby displaying potent anti-lymphangiogenic activity *in vivo*. These mechanisms of endothelial repulsion are common in blood endothelial cells (Sakurai et al., 2010) but appear to be independent of ERK1/2 and AKT phosphorylation downstream of VEGF-C-VEGFR3 signaling in LECs. At the molecular level, Sema3E-PlexinD1 signaling in blood endothelial cells relies on the GTPase-activating protein activity of PlexinD1 to inactivate R-Ras and activate Arf6 to modulate the cytoskeleton and cellular adhesion (Sakurai et al., 2010). Recent findings have suggested that actin-depolymerizing factor cofilin and molecules interacting with CasLs are involved in the interaction between Sema-Plexin and the actin cytoskeleton (Hung and Terman, 2011). Further studies are warranted to determine the detailed molecular signaling involved in this process.

Our present study identified *Sema3e* expression in the pericardium and epicardium, especially around the aortic root. PlexinD1 is broadly expressed in the endothelium. Taken together with the phenotypes of the mutant mice, regional cross talk between the epicardium and endocardium via Sema3E-PlexinD1 signaling may regulate the formation and remodeling of vasculature around the aorta. However, it remains unknown how two specific orifices are selected from multiple connections into aortic sinuses through Sema3E-PlexinD1 signaling, necessitating further study. *Sema3e* is also expressed in the ventricular epicardium. Thus, Sema3E-PlexinD1 signaling may affect sinus venosus- and epicardium-derived CVs. To test this possibility, sinus venosus- and epicardium-restricted *Sema3e* mutant mice would be necessary.

The present study further revealed the possible involvement of Sema3E-PlexinD1 signaling in pathological lymphangiogenesis and functional outcomes in post-ischemic myocardial injury using human recombinant PlexinD1 protein. PlexinD1 binds to Sema3E and blocks its effect. Given that coronary endothelial cells also express PlexinD1, the beneficial effect of Sema3E inhibition in post-MI hearts may arise from lymphangiogenesis, as well as from angiogenesis. Recent findings suggest that although Sema3C mainly interacts with PlexinD1 in an Nrp-dependent manner, it could directly interact with PlexinD1, forming complexes with PlexinA4 (Smolkin et al., 2018). Therefore, the effect of PlexinD1 may arise in a part from interaction with Sema3C. Recently, lymphangiogenesis has been implicated in various pathophysiological processes, including micro-edema, fibrosis after MI, and heart failure. Indeed, the new cardiac lymphatic vessels formed after MI remove excess fluid, cytokines, and cell debris and regulate the immune reaction in the injured area, resulting in the stabilization of scar tissue and improvements in cardiac function (Goichberg, 2016; Henri et al., 2016). Sema3E-PlexinD1 signaling may modulate these lymphangiogenic responses by antagonizing other semaphorin ligands and/or regional lymphangiogenic factors, including VEGF-C (Klotz et al., 2015). Thus, the present study provides mechanistic insights into post-MI lymphangiogenesis by identifying Sema3E-PlexinD1 signaling as a key participant. Additionally, Sema3E is known to act on PlexinD1-expressing monocytes/macrophages and modulate immune responses (Shimizu et al., 2013), which may partially explain the effect of Sema3E-PlexinD1 inactivation. Future studies are needed to dissect the contributions of each protein and cell type to this beneficial effect. Nevertheless, the developmental role of Sema3E-PlexinD1 signaling in cardiac vessel formation was extrapolated to pathological processes after MI, and strategies that interfere with Sema3E-PlexinD1 signaling may represent a therapeutic target for improving lymphatic development coupled with immune regulation.

In summary, Sema3E-PlexinD1 signaling has important functions in CA development and pathological processes associated with MI through lymphangiogenic mechanisms. Further characterization of the molecular processes that control the activity of Sema3E-PlexinD1 signaling will provide a fundamental basis for future therapeutic interventions to regenerate the cardiac vasculature and promote effective cardiac repair.

Limitations of the study

The limitations of this study are mainly related to ambiguity of cell types responsible for Sema3E-PlexinD1 signaling. Although we speculate epicardium-derived Sema3E is responsible for remodeling of vasculature around the aorta, definite evidence should be obtained by conditional Sema3E deletion. It is also true for the role of Sema3E-PlexinD1 in adult myocardial infarction, in which the source of Sema3E is likely different from the case of embryonic coronary development. Thus, *Sema3e* conditional knockout mice crossed with cell type-specific Cre mice would be expected to dissect more specific roles of Sema3E-PlexinD1 signaling in lymphatic vessel and coronary artery development and diseases in the future. In addition, macrophage/monocyte-specific Cre mice crossed with *Plexind1* conditional knockout mice would be beneficial to explore the possible involvement of immune components such as macrophages/monocytes in the pathophysiology of myocardial infarction.

Resource availability

Lead contact

Further information and requests for resources and reagents should be directed to and will be fulfilled by the lead contact, Kazuaki Maruyama (k.maruyama0608@gmail.com) or Hiroki Kurihara (kuri-tky@umin.net).

Materials availability

All data and materials associated with this study are available in the main text or the Supplemental Information.

METHODS

All methods can be found in the accompanying transparent methods supplemental file.

SUPPLEMENTAL INFORMATION

Supplemental information can be found online at https://doi.org/10.1016/j.isci.2021.102305.

ACKNOWLEDGMENTS

We thank all the lab members for participating in helpful discussions. We also thank Tetsuro Watabe (Tokyo Medical and Dental University) and Yasuhiro Yoshimatsu (Niigata University) for advises for the *in vitro* experiments. We also thank Xin Geng, YenChun Ho, Boksik Cha, Md. Riaj Mahamud, Lijuan Chen, and R. Sathish Srinivasan (Oklahoma Medical Research Foundation) for advices for experimental procedures. This work was supported in part by Grants-in-Aid for Scientific Research from the Ministry of Education, Culture, Sports, Science and Technology, Japan (19H01048 to H. K. and 20K17072 to K. M.); the Platform for Dynamic Approaches to Living System from the Ministry of Education, Culture, Sports, Science and Technology, Japan; and Core Research for Evolutional Science and Technology (CREST) of the Japan Science and Technology Agency (JST), Japan (JPMJCR13W2).

AUTHOR CONTRIBUTION

K.M., Y.A., S.M.-T., and H.K. conceived the study and designed the experiments. K.M. performed the majority of the experiments. K.N. implemented the cardiac injury model, and K.M. and H.N. performed the histological analysis. K.Y. performed echocardiography. A.U., Y.Y., and F.M. contributed to the mutant mice. Y.K. and Y.U. helped with data analyses. K.M., S.M.-T., M.K.S., and H.K. coordinated the experimental work, analyzed the data, and wrote the manuscript, with contributions from all authors.

DECLARATION OF INTERESTS

The authors declare no competing interests.

Received: April 14, 2020
Revised: February 28, 2021
Accepted: March 10, 2021
Published: April 23, 2021

REFERENCES

Adams, R.H., and Alitalo, K. (2007). Molecular regulation of angiogenesis and lymphangiogenesis. Nat. Rev. Mol. Cell Biol. *8*, 464–478, https://doi.org/10.1038/nrm2183.

Aghajanian, H., Choi, C., Ho, V.C., Gupta, M., Singh, M.K., and Epstein, J.A. (2014). Semaphorin 3d and semaphorin 3e direct endothelial motility through distinct molecular signaling pathways. J. Biol. Chem. *289*, 17971–17979, https://doi.org/10.1074/jbc.m113.544833.

Ando, K., Nakajima, Y., Yamagishi, T., Yamamoto, S., and Nakamura, H. (2004). Development of proximal coronary arteries in quail embryonic heart. Circ. Res. *94*, 346–352, https://doi.org/10.1161/01.res.0000112963.79064.09.

Angelini, P. (2007). Coronary artery anomalies. Circulation *115*, 1296–1305, https://doi.org/10.1161/circulationaha.106.618082.

Behar, O., Golden, J.A., Mashimo, H., Schoen, F.J., and Fishman, M.C. (1996). Semaphorin III is needed for normal patterning and growth of nerves, bones and heart. Nature *383*, 525–528, https://doi.org/10.1038/383525a0.

Bogers, A.J.J.C., Groot, A.C.G., Poelmann, R.E., Péault, B.M., and Huysmans, H.A. (1989). Development of the origin of the coronary arteries, a matter of ingrowth or outgrowth? Anat. Embryol. *180*, 437–441, https://doi.org/10.1007/bf00305118.

Bonet, F., Pereira, P.N.G., Bover, O., Marques, S., Inácio, J.M., and Belo, J.A. (2018). CCBE1 is required for coronary vessel development and proper coronary artery stem formation in the mouse heart. Dev. Dyn. *247*, 1135–1145, https://doi.org/10.1002/dvdy.24670.

Bouvrée, K., Brunet, I., Toro, R.D., Gordon, E., Prahst, C., Cristofaro, B., Mathivet, T., Xu, Y., Soueid, J., Fortuna, V., et al. (2012). Semaphorin3A, Neuropilin-1, and PlexinA1 are required for lymphatic valve formation. Circ. Res. *111*, 437–445, https://doi.org/10.1161/circresaha.112.269316.

Casazza, A., Finisguerra, V., Capparuccia, L., Camperi, A., Swiercz, J.M., Rizzolio, S., Rolny, C., Christensen, C., Bertotti, A., Sarotto, I., et al. (2010). Sema3E-Plexin D1 signaling drives human cancer cell invasiveness and metastatic spreading in mice. J. Clin. Invest. *120*, 2684–2698, https://doi.org/10.1172/jci42118.

Chen, Heidi I., Poduri, A., Numi, H., Kivela, R., Saharinen, P., McKay, A.S., Raftrey, B., Churko, J., Tian, X., Zhou, B., et al. (2014a). VEGF-C and aortic cardiomyocytes guide coronary artery stem development. J. Clin. Invest. *124*, 4899–4914, https://doi.org/10.1172/jci77483.

Chen, Heidi I., Sharma, B., Akerberg, B.N., Numi, H.J., Kivelä, R., Saharinen, P., Aghajanian, H., McKay, A.S., Bogard, P.E., Chang, A.H., et al. (2014b). The sinus venosus contributes to coronary vasculature through VEGFC-stimulated angiogenesis. Dev. Camb. Engl. *141*, 4500–4512, https://doi.org/10.1242/dev.113639.

Corà, D., Astanina, E., Giraudo, E., and Bussolino, F. (2014). Semaphorins in cardiovascular medicine. Trends Mol. Med. *20*, 589–598, https://doi.org/10.1016/j.molmed.2014.07.005.

Epstein, J.A., Aghajanian, H., and Singh, M.K. (2015). Semaphorin signaling in cardiovascular development. Cell Metab. *21*, 163–173, https://doi.org/10.1016/j.cmet.2014.12.015.

Feiner, L., Webber, A.L., Brown, C.B., Lu, M.M., Jia, L., Feinstein, P., Mombaerts, P., Epstein, J.A., and Raper, J.A. (2001). Targeted disruption of semaphorin 3C leads to persistent truncus arteriosus and aortic arch interruption. Dev. Camb. Engl. *128*, 3061–3070.

Fukushima, Y., Okada, M., Kataoka, H., Hirashima, M., Yoshida, Y., Mann, F., Gomi, F., Nishida, K., Nishikawa, S.-I., and Uemura, A. (2011). Sema3E-PlexinD1 signaling selectively suppresses disoriented angiogenesis in ischemic retinopathy in mice. J. Clin. Invest. *121*, 1974–1985, https://doi.org/10.1172/jci44900.

Gitler, A.D., Lu, M.M., and Epstein, J.A. (2004). PlexinD1 and semaphorin signaling are required in endothelial cells for cardiovascular development. Dev. Cell *7*, 107–116, https://doi.org/10.1016/j.devcel.2004.06.002.

Goichberg, P. (2016). Therapeutic lymphangiogenesis after myocardial infarction: vascular endothelial growth factor-C paves the way. J. Thorac. Dis. *8*, 1904–1907, https://doi.org/10.21037/jtd.2016.07.34.

Gu, C., Rodriguez, E.R., Reimert, D.V., Shu, T., Fritzsch, B., Richards, L.J., Kolodkin, A.L., and Ginty, D.D. (2003). Neuropilin-1 conveys semaphorin and VEGF signaling during neural and cardiovascular development. Dev. Cell *5*, 45–57, https://doi.org/10.1016/s1534-5807(03)00169-2.

Gu, C., Yoshida, Y., Livet, J., Reimert, D.V., Mann, F., Merte, J., Henderson, C.E., Jessell, T.M., Kolodkin, A.L., and Ginty, D.D. (2005). Semaphorin 3E and plexin-D1 control vascular pattern independently of neuropilins. Science *307*, 265–268, https://doi.org/10.1126/science.1105416.

Hamm, M.J., Kirchmaier, B.C., and Herzog, W. (2016). Sema3d controls collective endothelial cell migration by distinct mechanisms via Nrp1 and PlxnD1Sema3d regulates collective cell migration. J. Cell Biol. *215*, 415–430, https://doi.org/10.1083/jcb.201603100.

Hauser, M. (2005). Congenital anomalies of the coronary arteries. Heart *91*, 1240–1245, https://doi.org/10.1136/hrt.2004.057299.

Henri, O., Pouehe, C., Houssari, M., Galas, L., Nicol, L., Edwards-Lévy, F., Henry, J.-P., Dumesnil, A., Boukhalfa, I., Banquet, S., et al. (2016). Selective stimulation of cardiac lymphangiogenesis reduces myocardial edema and fibrosis leading to improved cardiac function following myocardial infarction. Circulation *133*, 1484–1497, https://doi.org/10.1161/circulationaha.115.020143.

Hung, R.-J., and Terman, J.R. (2011). Extracellular inhibitors, repellents, and semaphorin/plexin/MICAL-mediated actin filament disassembly. Cytoskelet Hoboken N. J. *68*, 415–433, https://doi.org/10.1002/cm.20527.

Hung, R.-J., Yazdani, U., Yoon, J., Wu, H., Yang, T., Gupta, N., Huang, Z., Berkel, W.J.H.van, and Terman, J.R. (2010). Mical links semaphorins to F-actin disassembly. Nature *463*, 823–827, https://doi.org/10.1038/nature08724.

Ieda, M., Kanazawa, H., Kimura, K., Hattori, F., Ieda, Y., Taniguchi, M., Lee, J.-K., Matsumura, K., Tomita, Y., Miyoshi, S., et al. (2007). Sema3a maintains normal heart rhythm through sympathetic innervation patterning. Nat. Med. *13*, 604–612, https://doi.org/10.1038/nm1570.

Ivins, S., Chappell, J., Vernay, B., Suntharalingham, J., Martineau, A., Mohun, T.J., and Scambler, P.J. (2015). The CXCL12/CXCR4 Axis plays a critical role in coronary artery development. Dev. Cell *33*, 455–468, https://doi.org/10.1016/j.devcel.2015.03.026.

Katz, T.C., Singh, M.K., Degenhardt, K., Rivera-Feliciano, J., Johnson, R.L., Epstein, J.A., and Tabin, C.J. (2012). Distinct compartments of the proepicardial organ give rise to coronary vascular endothelial cells. Dev. Cell *22*, 639–650, https://doi.org/10.1016/j.devcel.2012.01.012.

Klotz, L., Norman, S., Vieira, J.M., Masters, M., Rohling, M., Dubé, K.N., Bollini, S., Matsuzaki, F., Carr, C.A., and Riley, P.R. (2015). Cardiac lymphatics are heterogeneous in origin and respond to injury. Nature *522*, 62, https://doi.org/10.1038/nature14483.

Kruger, R.P., Aurandt, J., and Guan, K.-L. (2005). Semaphorins command cells to move. Nat. Rev. Mol. Cell Biol. *6*, 789–800, https://doi.org/10.1038/nrm1740.

Liu, X., Uemura, A., Fukushima, Y., Yoshida, Y., and Hirashima, M. (2016). Semaphorin 3G provides a repulsive guidance cue to lymphatic endothelial cells via neuropilin-2/PlexinD1. Cell Rep. *17*, 2299–2311, https://doi.org/10.1016/j.celrep.2016.11.008.

Maruyama, K., Miyagawa-Tomita, S., Mizukami, K., Matsuzaki, F., and Kurihara, H. (2019). Isl1-expressing non-venous cell lineage contributes to cardiac lymphatic vessel development. Dev. Biol. *452*, 134–143, https://doi.org/10.1016/j.ydbio.2019.05.002.

Mehta, V., Pang, K.-L., Rozbesky, D., Nather, K., Keen, A., Lachowski, D., Kong, Y., Karia, D., Ameismeier, M., Huang, J., et al. (2020). The guidance receptor plexin D1 is a mechanosensor in endothelial cells. Nature *578*, 290–295, https://doi.org/10.1038/s41586-020-1979-4.

Mikawa, T., and Gourdie, R.G. (1996). Pericardial mesoderm generates a population of coronary smooth muscle cells migrating into the heart along with ingrowth of the epicardial organ. Dev. Biol. *174*, 221–232, https://doi.org/10.1006/dbio.1996.0068.

Moriya, J., Minamino, T., Tateno, K., Okada, S., Uemura, A., Shimizu, I., Yokoyama, M., Nojima, A., Okada, M., Koga, H., and Komuro, I. (2010). Inhibition of semaphorin as a novel strategy for therapeutic angiogenesis. Circ. Res. *106*, 391–398, https://doi.org/10.1161/circresaha.109.210815.

Pérez-Pomares, J.-M., Carmona, R., González-Iriarte, M., Atencia, G., Wessels, A., and Muñoz-Chápuli, R. (2002). Origin of coronary endothelial

cells from epicardial mesothelium in avian embryos. Int. J. Dev. Biol. *46*, 1005–1013.

Poelmann, R.E., Groot, A.C.G., Mentink, M.M., Bökenkamp, R., and Hogers, B. (1993). Development of the cardiac coronary vascular endothelium, studied with antiendothelial antibodies, in chicken-quail chimeras. Circ. Res. *73*, 559–568, https://doi.org/10.1161/01.res.73.3.559.

Red-Horse, K., Ueno, H., Weissman, I.L., and Krasnow, M.A. (2010). Coronary arteries form by developmental reprogramming of venous cells. Nature *464*, 549–553, https://doi.org/10.1038/nature08873.

Sakurai, A., Gavard, J., Annas-Linhares, Y., Basile, J.R., Amornphimoltham, P., Palmby, T.R., Yagi, H., Zhang, F., Randazzo, P.A., Li, X., et al. (2010). Semaphorin 3E initiates antiangiogenic signaling through plexin D1 by regulating Arf6 and R-ras. Mol. Cell Biol. *30*, 3086–3098, https://doi.org/10.1128/mcb.01652-09.

Sandireddy, R., Cibi, D.M., Gupta, P., Singh, A., Tee, N., Uemura, A., Epstein, J.A., and Singh, M.K. (2019). Semaphorin 3E/PlexinD1 signaling is required for cardiac ventricular compaction. JCI Insight *4*, e125908, https://doi.org/10.1172/jci.insight.125908.

Shimizu, I., Yoshida, Y., Moriya, J., Nojima, A., Uemura, A., Kobayashi, Y., and Minamino, T. (2013). Semaphorin3E-Induced inflammation contributes to insulin resistance in dietary obesity. Cell Metab. *18*, 491–504, https://doi.org/10.1016/j.cmet.2013.09.001.

Smolkin, T., Nir-Zvi, I., Duvshani, N., Mumblat, Y., Kessler, O., and Neufeld, G. (2018). Complexes of plexin-A4 and plexin-D1 convey semaphorin-3C signals to induce cytoskeletal collapse in the absence of neuropilins. J. Cell Sci. *131*, jcs208298, https://doi.org/10.1242/jcs.208298.

Tata, A., Stoppel, D.C., Hong, S., Ben-Zvi, A., Xie, T., and Gu, C. (2014). An image-based RNAi screen identifies SH3BP1 as a key effector of Semaphorin 3E-PlexinD1 signaling. J. Cell Biol. *205*, 573–590, https://doi.org/10.1083/jcb.201309004.

Théveniau-Ruissy, M., Dandonneau, M., Mesbah, K., Ghez, O., Mattei, M.-G., Miquerol, L., and Kelly, R.G. (2008). The del22q11.2 candidate gene Tbx1 controls regional outflow tract identity and coronary artery patterning. Circ. Res. *103*, 142–148, https://doi.org/10.1161/circresaha.108.172189.

Théveniau-Ruissy, M., Pérez-Pomares, J.-M., Parisot, P., Baldini, A., Miquerol, L., and Kelly, R.G. (2016). Coronary stem development in wild-type and Tbx1 null mouse hearts. Dev. Dyn. *245*, 445–459, https://doi.org/10.1002/dvdy.24380.

Tian, X., Hu, T., He, L., Zhang, H., Huang, X., Poelmann, R.E., Liu, W., Yang, Z., Yan, Y., Pu, W.T., and Zhou, B. (2013a). Peritruncal coronary endothelial cells contribute to proximal coronary artery stems and their aortic orifices in the mouse heart. PLoS One *8*, e80857, https://doi.org/10.1371/journal.pone.0080857.

Tian, X., Hu, T., Zhang, H., He, Lingjuan, Huang, X., Liu, Q., Yu, W., He, Liang, Yang, Zhongzhou, Zhang, Z., et al. (2013b). Subepicardial endothelial cells invade the embryonic ventricle wall to form coronary arteries. Cell Res. *23*, 1075–1090, https://doi.org/10.1038/cr.2013.83.

Toyofuku, T., Yabuki, M., Kamei, J., Kamei, M., Makino, N., Kumanogoh, A., and Hori, M. (2007). Semaphorin-4A, an activator for T-cell-mediated immunity, suppresses angiogenesis via Plexin-D1. EMBO J. *26*, 1373–1384, https://doi.org/10.1038/sj.emboj.7601589.

Toyofuku, T., Yoshida, J., Sugimoto, T., Yamamoto, M., Makino, N., Takamatsu, H., Takegahara, N., Suto, F., Hori, M., Fujisawa, H., et al. (2008). Repulsive and attractive semaphorins cooperate to direct the navigation of cardiac neural crest cells. Dev. Biol. *321*, 251–262, https://doi.org/10.1016/j.ydbio.2008.06.028.

Waldo, K.L., Willner, W., and Kirby, M.L. (1990). Origin of the proximal coronary artery stems and a review of ventricular vascularization in the chick embryo. Am. J. Anat. *188*, 109–120, https://doi.org/10.1002/aja.1001880202.

Wu, B., Zhang, Z., Lui, W., Chen, X., Wang, Y., Chamberlain, A.A., Moreno-Rodriguez, R.A., Markwald, R.R., O'Rourke, B.P., Sharp, D.J., et al. (2012). Endocardial cells form the coronary arteries by angiogenesis through myocardial-endocardial VEGF signaling. Cell *151*, 1083–1096, https://doi.org/10.1016/j.cell.2012.10.023.

Zhang, Y., Singh, M.K., Degenhardt, K.R., Lu, M.M., Bennett, J., Yoshida, Y., and Epstein, J.A. (2009). Tie2Cre-mediated inactivation of plexinD1 results in congenital heart, vascular and skeletal defects. Dev. Biol. *325*, 82–93, https://doi.org/10.1016/j.ydbio.2008.09.031.

iScience, Volume *24*

Supplemental information

Semaphorin3E-PlexinD1 signaling in coronary artery and lymphatic vessel development with clinical implications in myocardial recovery

Kazuaki Maruyama, Kazuaki Naemura, Yuichiro Arima, Yasunobu Uchijima, Hiroaki Nagao, Kenji Yoshihara, Manvendra K. Singh, Akiyoshi Uemura, Fumio Matsuzaki, Yutaka Yoshida, Yukiko Kurihara, Sachiko Miyagawa-Tomita, and Hiroki Kurihara

Figure S1

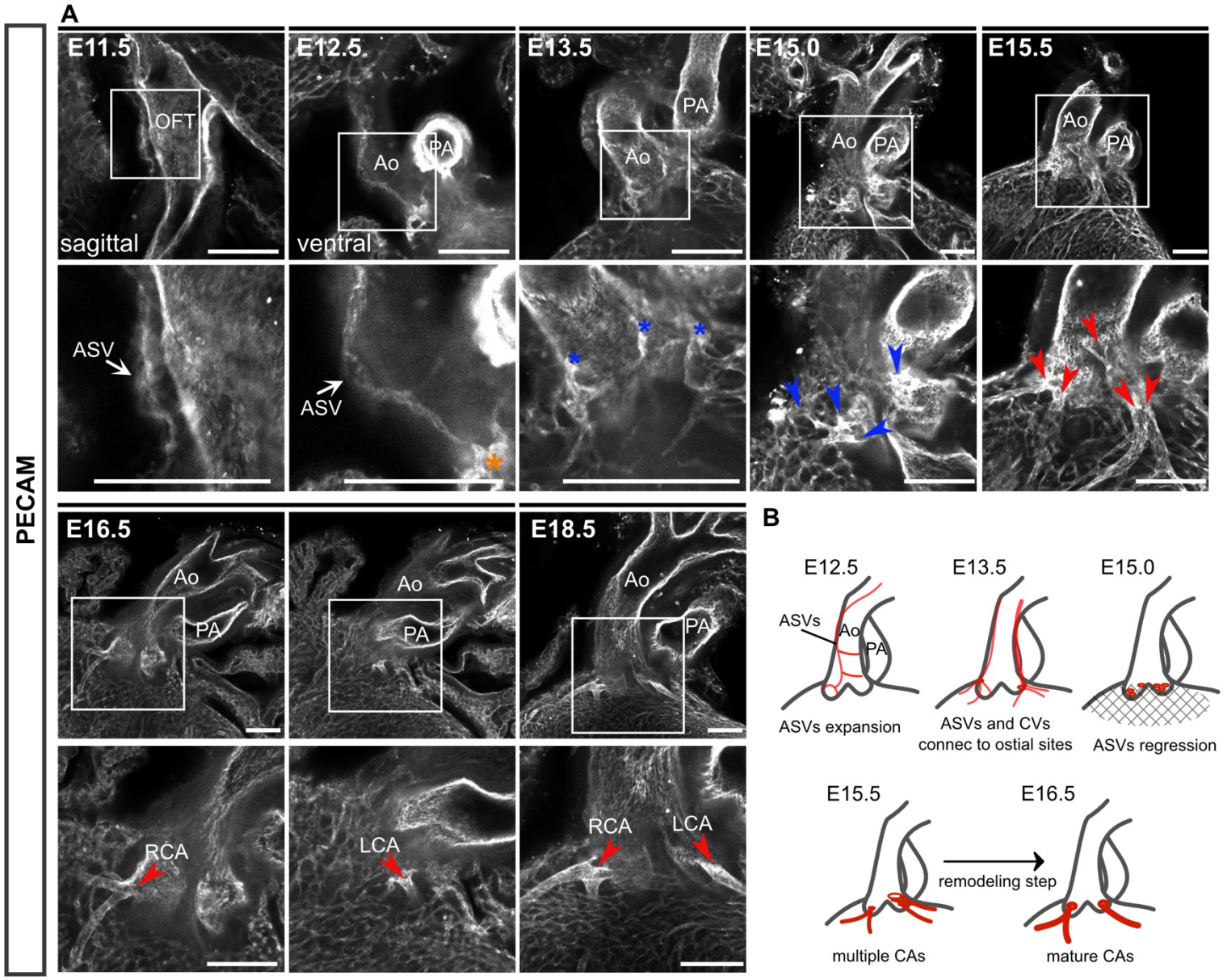
A
PECAM
E11.5
OFT
sagittal
E12.5
Ao
PA
ventral
E13.5
PA
Ao
E15.0
Ao
PA
E15.5
Ao
PA
ASV
ASV
E16.5
Ao
PA
E18.5
Ao
PA
RCA
LCA
RCA
LCA
B
E12.5
ASVs
Ao
PA
ASVs expansion
E13.5
ASVs and CVs
connec to ostial sites
E15.0
ASVs regression
E15.5
E16.5
remodeling step
multiple CAs
mature CAs

Figure S1. CA ostium development in wild type mice

(A) Whole-mount confocal images of wild type hearts labeled for PECAM. White arrows indicated ASVs. Orange asterisks indicated the ASVs connection site to the aortic lumen at E12.5. CVs grew and connected to the aortic sinuses at multiple sites (blue asterisks). These connections were increased at E15.0 (blue arrowheads). At E15.5, large connections formed between the aorta and CVs (red arrowheads). At E16.5, two mature ostia formed (red arrowheads) and maintained at E18.5 (red arrowheads). (**B**) Schematic representation of CA ostium development in wild type embryos. ASVs, aortic subepicardial vessels; CVs, coronary vessels. Ao, aorta; PA, pulmonary artery; RCA, right coronary artery; LCA, left coronary artery. Scale bars, 100 μm (**A**).

Figure S1, related to Figure 2

Figure S2

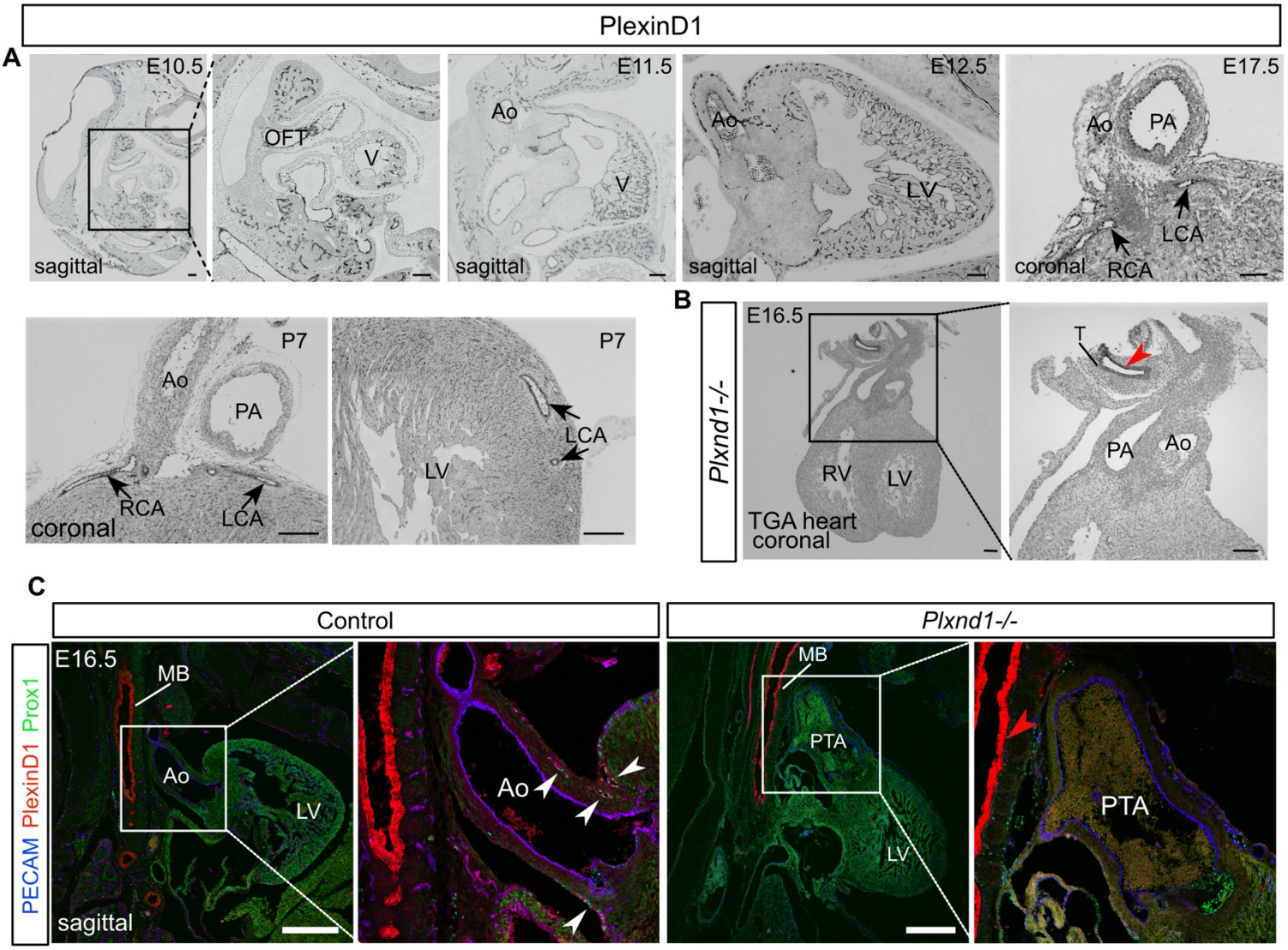
PlexinD1
A
E10.5
OFT
V
sagittal
E11.5
Ao
V
sagittal
E12.5
Ao
LV
sagittal
E17.5
Ao
PA
LCA
RCA
coronal
P7
Ao
PA
RCA
LCA
coronal
P7
LCA
LV
B
Plxnd1-/-
E16.5
RV
LV
TGA heart
coronal
T
PA
Ao
C
Control
Plxnd1-/-
PECAM PlexinD1 Prox1
E16.5
MB
Ao
LV
sagittal
Ao
MB
PTA
LV
PTA

Figure S2. PlexinD1 is expressed in blood and lymphatic endothelial cells

(A, B) Paraffin sections immunostained for PlexinD1 in the developing heart at the indicated embryonic and postnatal stages. PlexinD1 was expressed in the endocardium and the endothelium, including the CAs (black arrows). (**B**) In *Plxnd1*$^{-/-}$ hearts at E16.5, PlexinD1 was undetectable, except in the bronchial epithelium (red arrowhead). (**C**) Sagittal sections of control and *Plxnd1*$^{-/-}$ embryos labeled for PECAM, Prox1 and PlexinD1 at E16.5. PlexinD1 was detected in lymphatic vessels around the aorta and merged with PECAM and Prox1 in control embryos (white arrowheads), whereas PlexinD1 was undetectable in *Plxnd1*$^{-/-}$ embryos, except in the bronchial epithelium (red arrowhead). OFT, outflow tract; V, ventricle; Ao, aorta; LV, left ventricle; PA, pulmonary artery; RCA, right coronary artery; LCA, left coronary artery; RV, right ventricle; T, trachea; MB, main bronchus; PTA, persistent truncus arteriosus. Scale bars, 100 μm **(A, B)**, 500 μm (**C**).

Figure S2, related to Figure 3

Figure S3

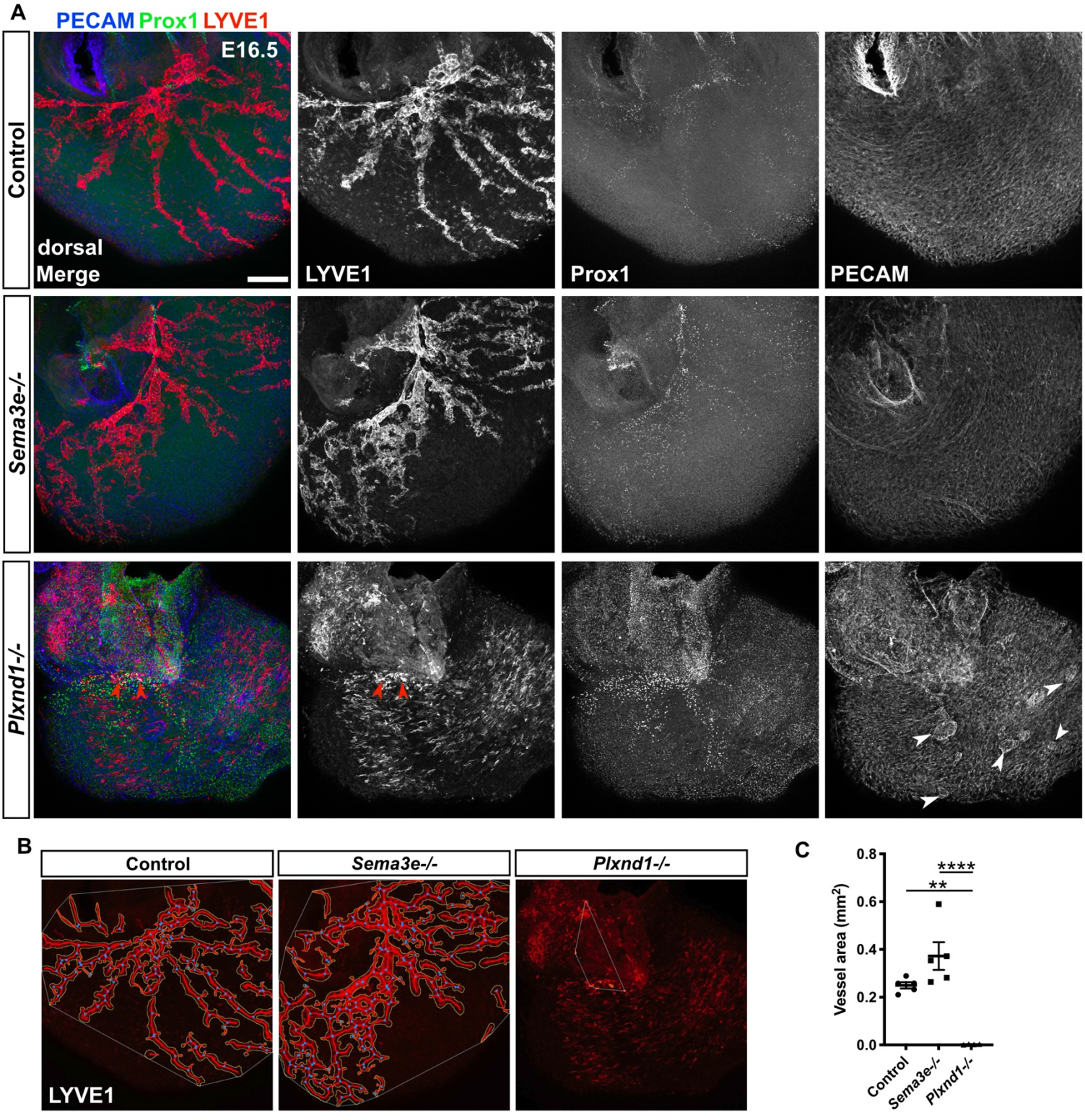
A
PECAM Prox1 LYVE1
Control
E16.5
dorsal
Merge
LYVE1
Prox1
PECAM
Sema3e-/-
Plxnd1-/-
B
Control
Sema3e-/-
Plxnd1-/-
LYVE1
C
Vessel area (mm2)
0.8
0.6
0.4
0.2
0.0
****
**
Control
Sema3e-/-
Plxnd1-/-

Figure S3. Effects of impaired Sema3E-PlexinD1 signaling on cardiac lymphatic vessel formation

(A) Whole-mount confocal images of control, *Sema3e*$^{-/-}$, or *Plxnd1*$^{-/-}$ hearts labeled for PECAM, Prox1, and LYVE1. In *Sema3e*$^{-/-}$ mice, hyperplastic PECAM^{+}/Prox1^{+}/LYVE1^{+} cardiac lymphatic vessels were observed. In contrast, PECAM^{+} ectopic CVs (white arrowheads) and Prox1^{+} lymphatic vessels with partial LYVE1 expression were observed in *Plxnd1*$^{-/-}$ mice (red arrowheads). (**B)** Whole-mount confocal images of control, *Sema3e*$^{-/-}$ or *Plxnd1*$^{-/-}$ hearts at E16.5 captured for AngioTool analyses. The tracing was depicted for LYVE1^{+} vessels (red) and branch points (blue) and enabled the quantitative assessment of vessel parameters. **(C)** Quantification of vessel area. CVs, coronary vessels. Each dot represents a value obtained from one sample. All the data are presented as the means±SEM, and statistical analyses were performed using a one-way ANOVA between groups and post hoc multiple comparisons using Bonferroni's test. * P<0.05, ** P<0.01, ****P<0.0001. Scale bars, 100 μm **(A)**.

Figure S3, related to Figure 4 and 5

Figure S4

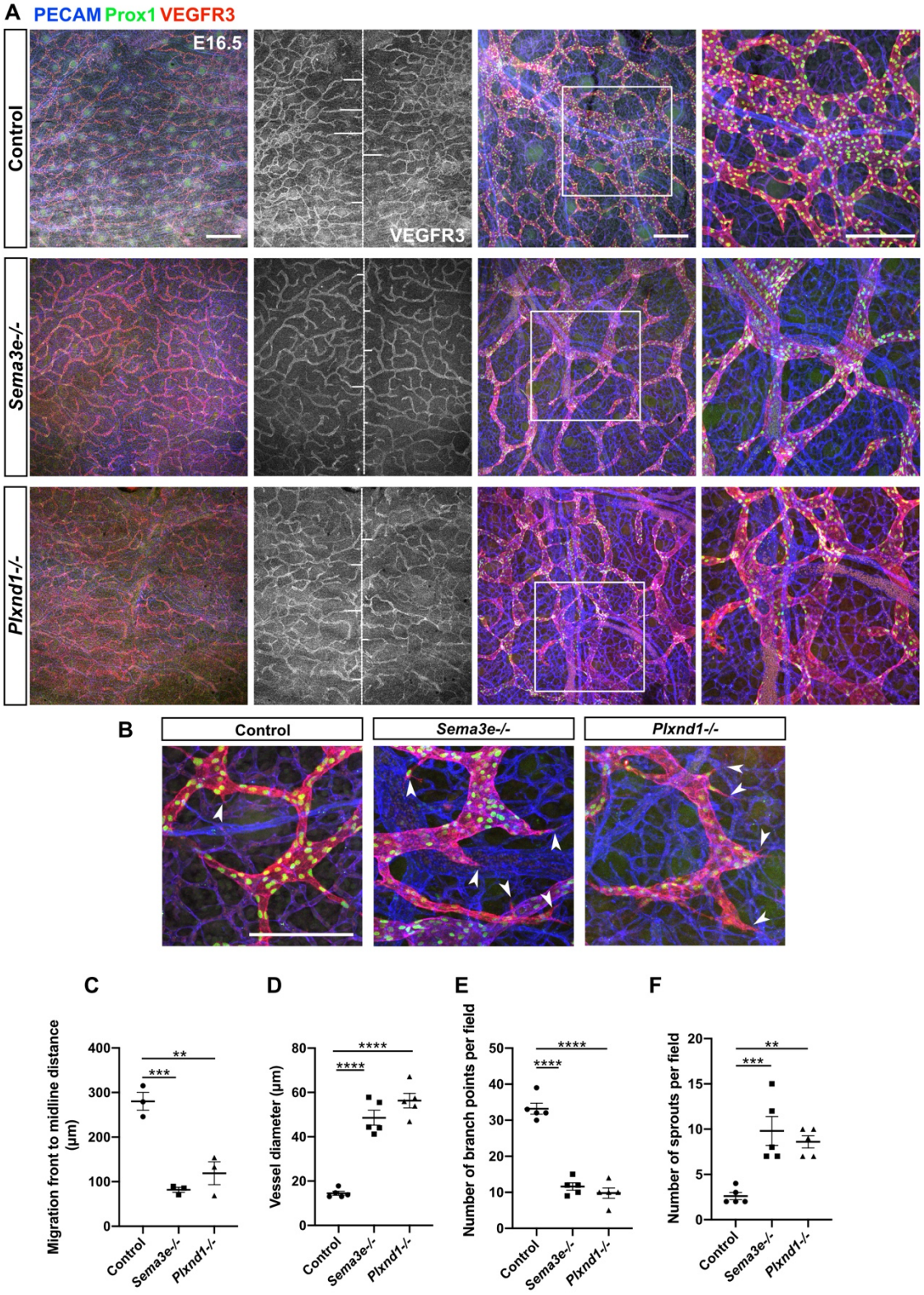
A
PECAM Prox1 VEGFR3
E16.5
Control
Sema3e-/-
Plxnd1-/-
VEGFR3
B
Control
Sema3e-/-
Plxnd1-/-
C
Migration front to midline distance (μm)
D
Vessel diameter (μm)
E
Number of branch points per field
F
Number of sprouts per field
Control
Sema3e-/-
Plxnd1-/-

Figure S4. *Sema3e*$^{-/-}$ embryos show dilated lymphatic vessels in the dorsal skin

(A, B) Whole-mount confocal images of control, *Sema3e*$^{-/-}$, or *Plxnd1*$^{-/-}$ dorsal skin labeled for PECAM, Prox1, and VEGFR3 at E16.5. In the dorsal skin, VEGFR3^{+} lymphatic vessels migrate from the two sides toward the midline (white dotted lines). White lines represent examples of migration front to midline distance. Boxed areas are magnified in the right panels. (**B**) *Sema3e*$^{-/-}$ and *Plxnd1*$^{-/-}$ mice showed an excessive number of sprouts (white arrowheads). (**C-F**) Quantification of distance from the migration front to midline (white lines in (**A**)), vessel diameter, number of branch points and number of sprouts (five points were counted in each sample). Each dot represents a value obtained from one sample. All the data are presented as the means±SEM, and statistical analyses were performed using a one-way ANOVA between groups and post hoc multiple comparisons using Bonferroni's test. ** P<0.01, *** P<0.001, **** P<0.0001. Scale bars, 500 μm (**A left panel**), 100 μm **(A right panels)**, 50 μm **(B)**.

Figure S4, related to Figure 4 and 5

Figure S5

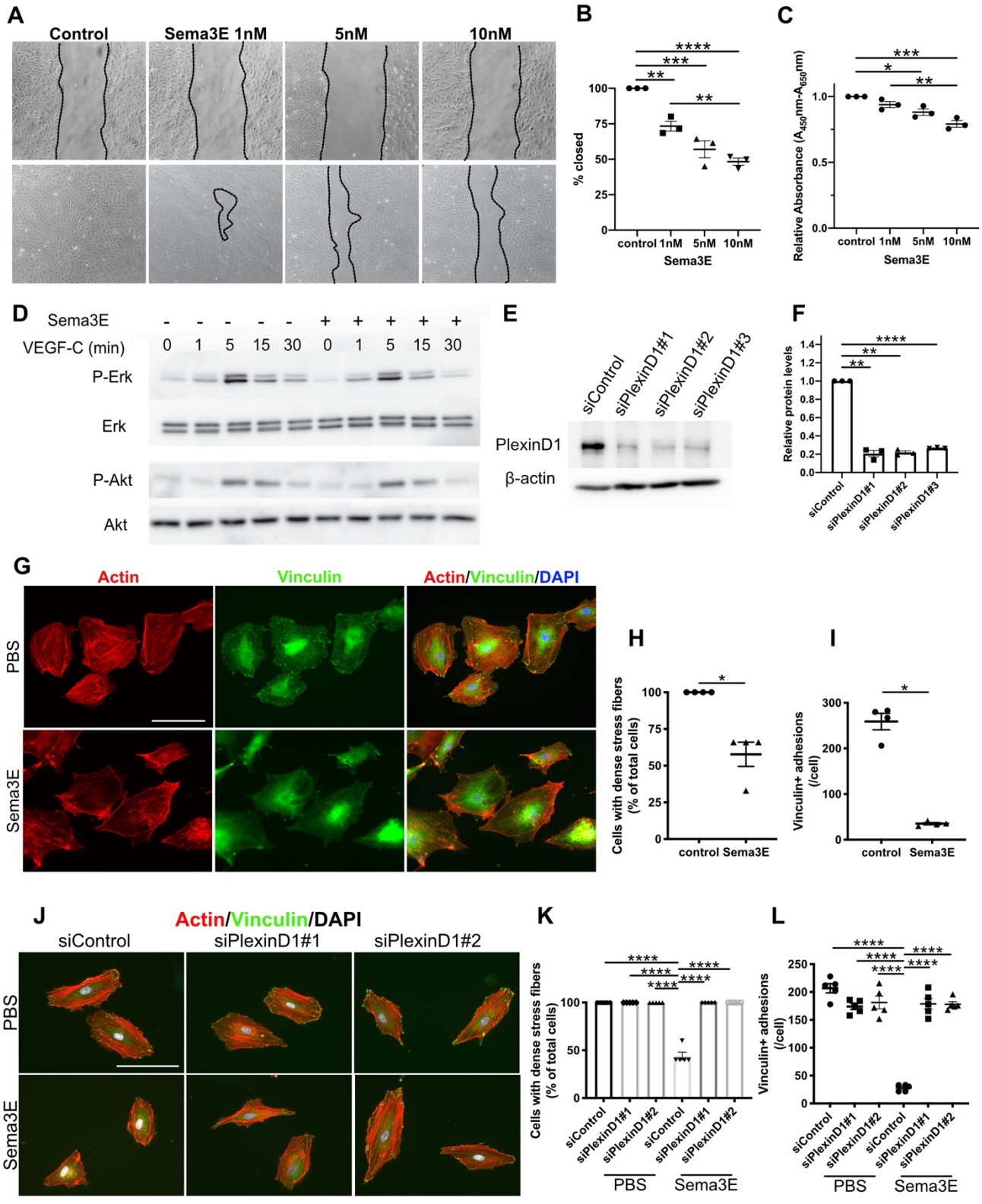
A
Control
Sema3E 1nM
5nM
10nM
B
% closed
control 1nM 5nM 10nM
Sema3E
C
Relative Absorbance (A450nm-A650nm)
control 1nM 5nM 10nM
Sema3E
D
Sema3E
VEGF-C (min)
0 1 5 15 30 0 1 5 15 30
P-Erk
Erk
P-Akt
Akt
E
siControl
siPlexinD1#1
siPlexinD1#2
siPlexinD1#3
PlexinD1
β-actin
F
Relative protein levels
siControl
siPlexinD1#1
siPlexinD1#2
siPlexinD1#3
G
Actin
Vinculin
Actin/Vinculin/DAPI
PBS
Sema3E
H
Cells with dense stress fibers (% of total cells)
control Sema3E
I
Vinculin+ adhesions (/cell)
control Sema3E
J
Actin/Vinculin/DAPI
siControl
siPlexinD1#1
siPlexinD1#2
PBS
Sema3E
K
Cells with dense stress fibers (% of total cells)
siControl
siPlexinD1#1
siPlexinD1#2
PBS
Sema3E
L
Vinculin+ adhesions (/cell)
siControl
siPlexinD1#1
siPlexinD1#2
PBS
Sema3E

Figure S5. Sema3E induces lymphatic endothelial cell retraction

(**A**) Wound healing assay in the absence or presence of recombinant Sema3E at indicated concentrations (1 nM, 5 nM and 10 nM). Percent closed area was quantified in (**B**) (n=3, biological replicates in all conditions). (**C**) MTT cell proliferation assay for the control or recombinant Sema3E treated HLECs. (**D**) LEC phosphorylation assay. HLECs exposed for 30 min to control medium or recombinant Sema3E (10 nM) were further cultured in the absence or presence of VEGF-C (200 ng/mL) for the indicated times, followed by lysis for western blotting of phosphorylated Akt (P-Akt), total Akt, phosphorylated Erk (P-Erk), and total Erk (n=5, biological replicates in all conditions). (**E, F**) Confirmation of PlexinD1 knockdown by western blotting with PlexinD1 antibody. Stealth siRNAs targeting three different regions of the PlexinD1 transcript. HLECs exposed to control or siPlexinD1 were further cultured for 72 h, followed by lysis for western blotting of PlexinD1 (n=3, biological replicates in all conditions). (**G**) HLECs were exposed to 10 nM recombinant Sema3E or PBS for 1 h and subsequently stained for F-actin, vinculin and DAPI. Quantification of the percentage of HLECs displaying an absence of dense actin stress fibers (**H**) or vinculin positive focal adhesions (**I**) (n=4, biological replicates in all conditions; 3 cells were analyzed in all conditions). (**J**) HLECs were transfected with control siRNA or siPlexinD1 and cultured to 80% confluency. Cells were passaged and seeded at 15% confluency. The following day, HLECs were exposed to PBS or 10 nM Sema3E for 1 h and stained for F-actin, vinculin, and DAPI. Vinculin^{+} focal adhesions and cells with dense stress fibers were quantified in (**K, L**) (n=5, biological replicates in all conditions; 5 cells were counted in each conditions). All results are expressed as the means ± SEM, and statistical analyses were performed using a one-way ANOVA between groups, post hoc multiple comparisons, Bonferroni's test. * P<0.05, ** P<0.01, *** P<0.001, **** P<0.0001. Scale bars, 100 μm **(G, J)**.

Figure S5, related to Figure 6

Figure S6

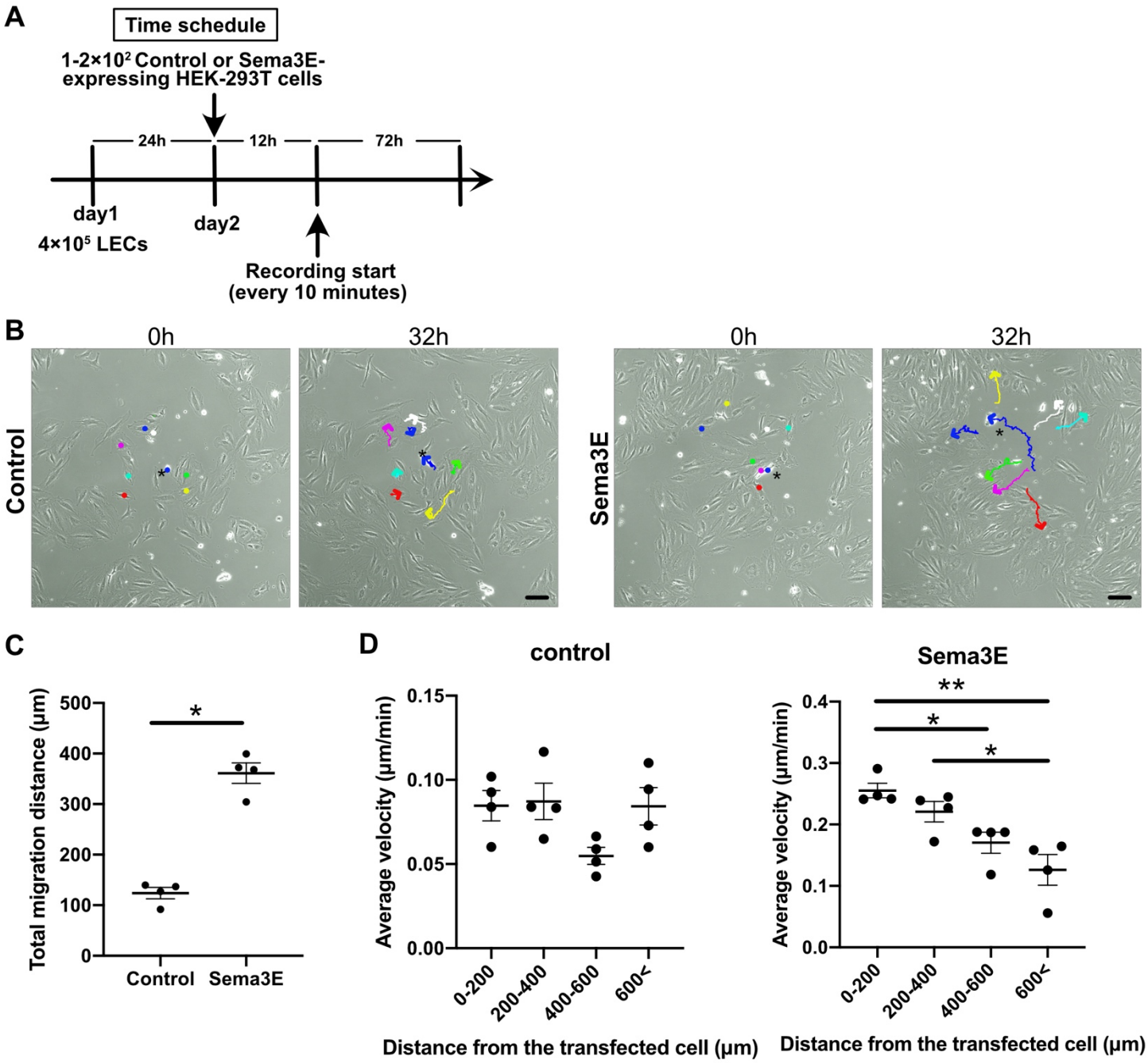
A
Time schedule
1-2×10² Control or Sema3E-expressing HEK-293T cells
24h
12h
72h
day1
4×10⁵ LECs
day2
Recording start
(every 10 minutes)
B
0h
32h
Control
Sema3E
C
Total migration distance (μm)
Control
Sema3E
D
control
Sema3E
Average velocity (μm/min)
0-200
200-400
400-600
600<
Distance from the transfected cell (μm)

Figure S6. Time-lapse imaging of the repelling effect of Sema3E-expressing cells on lymphatic endothelial cells

(**A**) Time schedule for the time-lapse imaging. (**B**) Control HEK-293T cells transfected with pFLAG-T2A-EGFP vectors (control) or HEK-293T cells transfected with pFLAG-Sema3E-T2A-EGFP (Sema3E) were seeded on top of HLECs and incubated for an additional 72 h. Tracks representing the migration paths of individual HLECs incubated for 32 h. Live-images were captured every 10 min. (**C, D**) Quantification of total length and average velocity in each condition (n=4, biological replicates in all conditions; 5-8 cells were tracked in each condition). All results are expressed as the means ± SEM, and statistical analyses were performed using a one-way ANOVA between groups, post hoc multiple comparisons, Bonferroni's test. * $P<0.05$, ** $P<0.01$. Scale bars, 100 μm **(B)**.

Figure S6, related to Figure 6

Figure S7

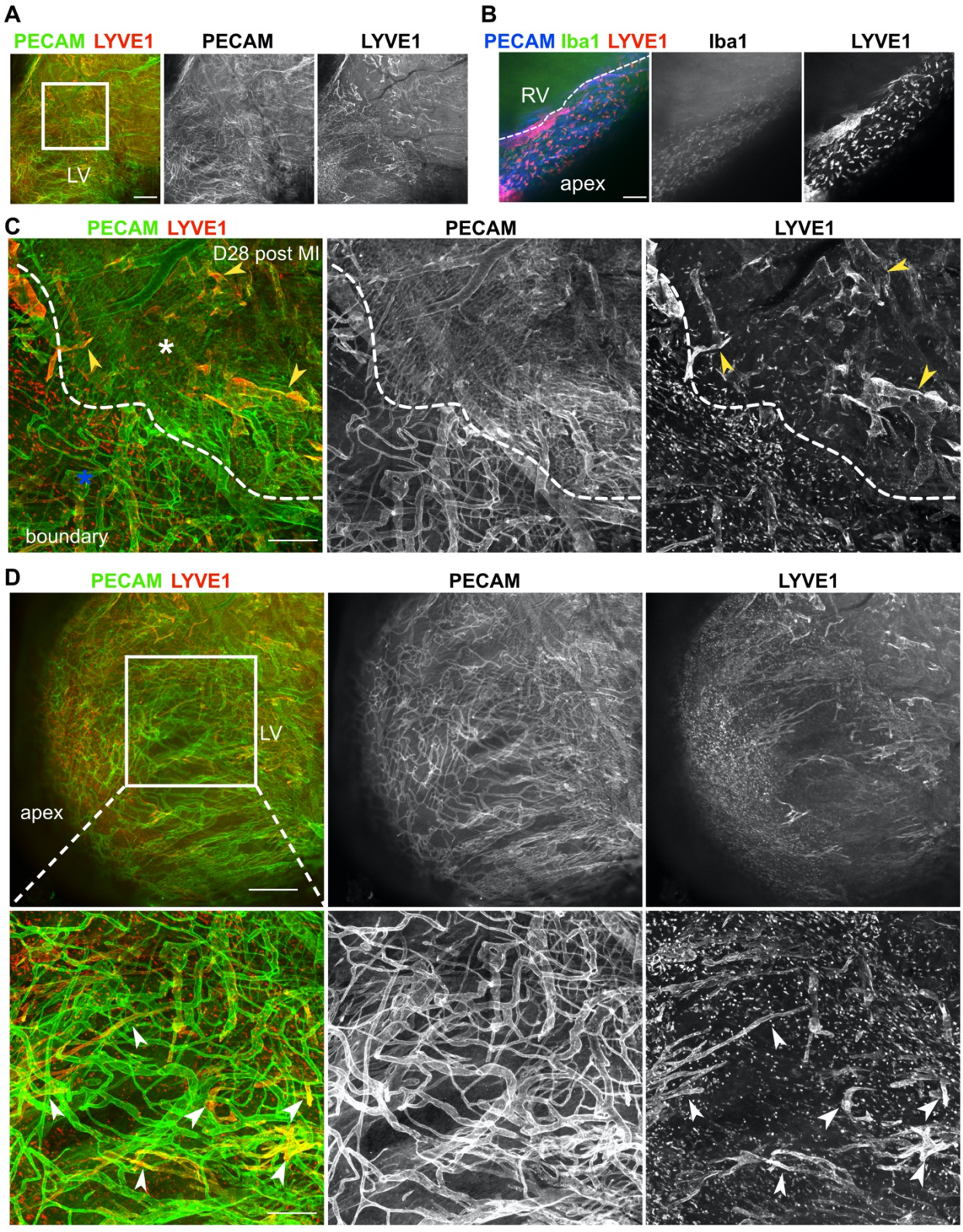
A
PECAM LYVE1
PECAM
LYVE1
LV
B
PECAM Iba1 LYVE1
Iba1
LYVE1
RV
apex
C
PECAM LYVE1
PECAM
LYVE1
D28 post MI
boundary
D
PECAM LYVE1
PECAM
LYVE1
LV
apex

Figure S7. Myocardial infarction induces substantial cardiac lymphangiogenesis and vascular remodeling

(A, C, D) Whole-mount confocal images of infarcted hearts stained for PECAM and LYVE1 on day 28 after MI. **(B)** $LYVE1^+$ cells colocalized with the macrophage marker Iba1 in the infarction area (white dotted line represents the boundary between the infarcted area and the non-infarcted area). **(C)** Boxed areas in **(A)** are magnified in **(C)**. White dotted lines represent the boundary between the infarcted area (blue asterisk) and the non-infarcted area (white asterisk). $LYVE1^+$ reactive lymphangiogenesis was observed in the non-infarcted area (yellow arrowheads). In contrast, $LYVE1^+$ macrophage infiltration was observed in the infarcted area. **(D)** A substantial number of $LYVE1^+$ macrophages had migrated into the infarcted area, and weak lymphangiogenesis was observed (white arrowheads). LV, left ventricle; RV, right ventricle; MI, myocardial infarction. Scale bars, 500 μm **(A, B and D top panels)**, 100 μm **(C and D bottom panels)**.

Figure S7, related to Figure 7

Figure S8

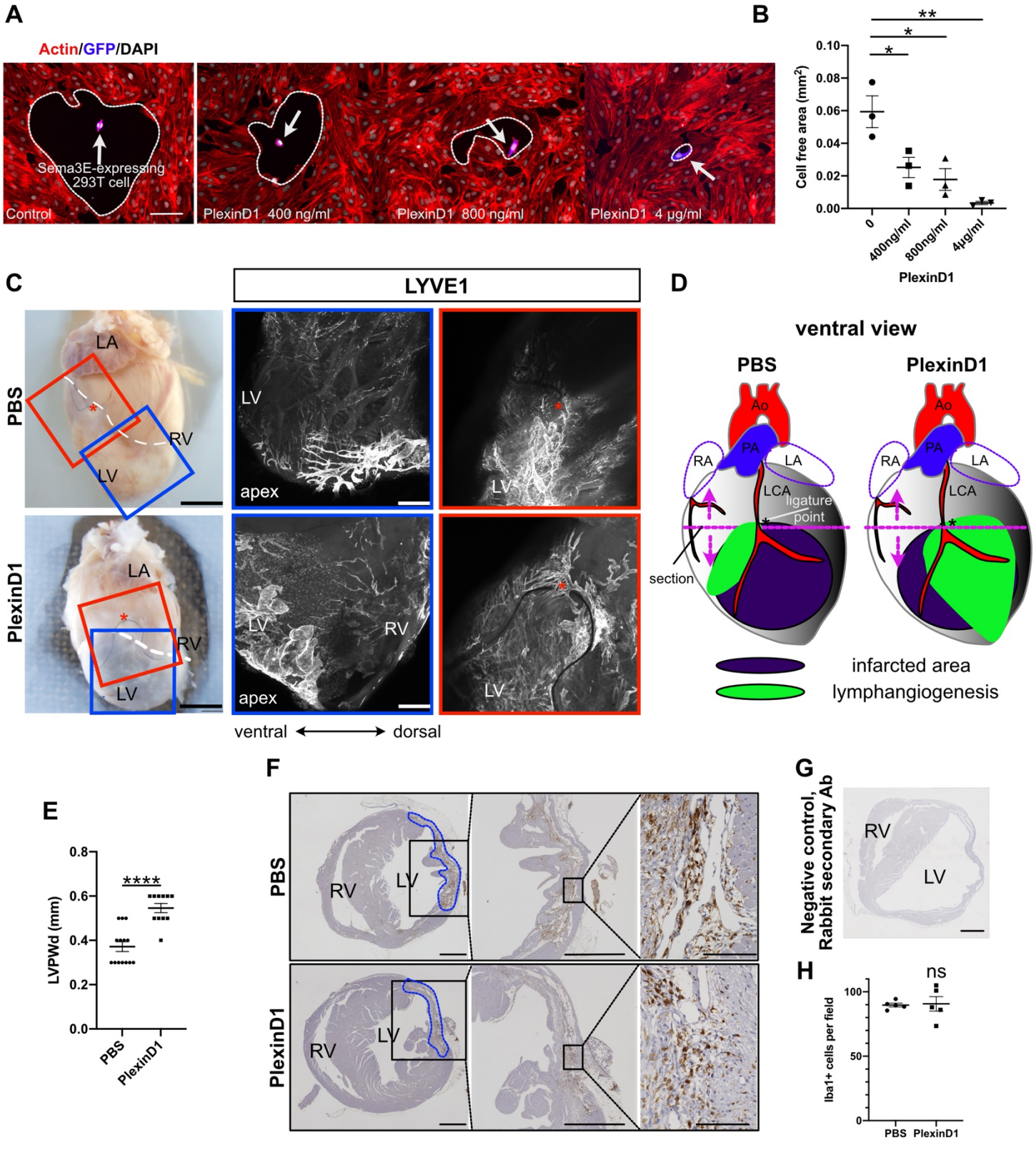
A
Actin/GFP/DAPI
Sema3E-expressing 293T cell
Control
PlexinD1 400 ng/ml
PlexinD1 800 ng/ml
PlexinD1 4 µg/ml
B
Cell free area (mm²)
0.10
0.08
0.06
0.04
0.02
0.00
0
400ng/ml
800ng/ml
4µg/ml
PlexinD1
C
LYVE1
PBS
PlexinD1
LA
RV
LV
apex
ventral ⟷ dorsal
D
ventral view
PBS
PlexinD1
Ao
PA
RA
LA
LCA
ligature point
section
infarcted area
lymphangiogenesis
E
LVPWd (mm)
0.8
0.6
0.4
0.2
0.0
****
PBS
PlexinD1
F
PBS
PlexinD1
RV
LV
G
Negative control, Rabbit secondary Ab
RV
LV
H
Iba1+ cells per field
100
50
0
ns
PBS
PlexinD1

Figure S8. Inhibition of Sema3E-PlexinD1 signaling stimulates angiogenesis and lymphangiogenesis

(A) LEC repulsive assay in the absence or presence of recombinant PlexinD1 at the indicated concentrations (400 ng/mL, 800 ng/mL, and 4 μg/mL). White dotted lines represent LEC free area and white arrows represent Sema3E-expressing HEK-293T cells. LEC free area was quantified in (**B**) (n=3, biological replicates in all conditions; 5-7 regions were counted in each condition). **(C)** Gross appearance and whole-mount confocal images of hearts treated with PBS or recombinant PlexinD1 (PlexinD1), stained for LYVE1 28 days after MI (red asterisks indicate the ligature suture points and white dotted lines represent the boundary between the infarcted area and non-infarcted area). Boxed areas in the left panels are magnified in the right panels. The $LYVE1^+$ lymphatic vessel area is schematically presented in **(D)**. (**E**) Evaluation of left ventricle posterior thickness at diastole (LVPWd). **(F, G)** Paraffin sections obtained from PBS- or recombinant PlexinD1-treated (PlexinD1) MI mice, immunostained for Iba1 or rabbit secondary antibody as a negative control. Blue dotted areas represent infarcted regions **(F).** The number of $Iba1^+$ macrophages was quantified in (**H**). LA, left atrium; RA, right atrium; LV, left ventricle; RV, right ventricle; MI, myocardial infarction; Ab, antibody. Each dot represents a value obtained from one sample. All results are expressed as the means ± SEM, and statistical analyses were performed using a one-way ANOVA between groups, and post hoc multiple comparisons using Bonferroni's test (**B**), or non-parametric Mann-Whitney's *u*-test (**H**). ns, $P \geq 0.05$, * $P<0.05$, ** $P<0.01$, **** $P<0.0001$. Scale bars, 2 mm (**C left panels**), 1 mm (**F left and middle panels**), 500 μm (**C middle panels**), 100 μm (**A**, **F right panels**).

Figure S8, related to Figure 7

TRANSPARENT METHODS

Mouse strains

The following mouse strains were employed: *Sema3e*$^{-/-}$ and *Plxnd1*$^{-/-}$ mice(Gu et al., 2005). *Sema3e*$^{+/+}$ and *Sema3e*$^{+/-}$ mice were used as controls; similarly, for *the Plxnd1* genotypes. The genotypes were determined by PCR using tail-tip or amnion DNA, and the specific primers are listed in Table 1. The mice were housed in an environmentally controlled room at 23±2°C, with a relative humidity of 50%–60% under a 12-h light:12-h dark cycle. The embryonic stages were determined by timed mating; the day the plug was observed was designated embryonic day (E) 0.5. Both female and male animals at E11.5 to E18.5 and postnatal day 7 were randomly subjected to the experiments and there was no difference in experimental results due to sex differences. All animal experiments were approved by the University of Tokyo and Tokyo Women's Medical University Animal Care and Use Committee and were performed in accordance with institutional guidelines.

Immunohistochemistry, histology, confocal imaging, and quantification

For histological analyses, hearts and embryos were collected, fixed with 4% paraformaldehyde (PFA), stored in PBS, embedded in paraffin (Kanto Chemical, Tokyo, Japan) or OCT (Sakura Finetek). Paraffin sections (4 μm) were stained with hematoxylin (Merck) and eosin (Kanto Chemical, Tokyo, Japan). Immunofluorescence staining of 4-μm paraffin or 16-μm frozen sections was performed using primary antibodies against CD31 (553370, BD Pharmingen, 1:50), Prox1 (11-002, AngioBio, 1:200), Prox1 (AF2727, R&D Systems, 1:200), LYVE1 (AF2125, R&D Systems, 1:50), VEGFR-3 (AF743, R&D Systems, 1:50), GFP (GF090R, Nacalai Tesque, 1:1000), GFP (GFP-RB-AF2020, FRL, 1:250), PlexinD1 (AF4160, R&D Systems, 1:100), vinculin (V9131, Merck, 1:200), endomucin (14-5851-85, eBioscience, 1:100), and Iba1 (019-19741, WAKO, 1:500). Alexa Fluor-conjugated secondary antibodies (Abcam, 1:200) were subsequently applied. The same protocol was utilized for whole-mounted hearts and embryos, but the primary and secondary antibody incubations were extended to two nights. Whole-mount 3,39-diaminobenzidine (DAB) staining was performed on embryonic and postnatal hearts using the Vectastain ABC System (Vector Laboratories). Images of the immunofluorescence staining were captured using a Nikon C2 confocal microscope. Maximum intensity z-projections of whole or sectioned hearts or skin were acquired using both the tiling and z-stack functions. The thickness of the z-projections was 10 μm for whole and 1 or 2 μm for sectioned samples. DAB staining was observed under a Keyence BZ-X700 microscope. All images were processed using ImageJ and Nikon NIS Elements software. Vessel areas were calculated using AngioTool (Zudaire et al., 2011).

Cryosection *in situ* hybridization was performed as previously described (Asai et al., 2010). The *Sema3e* probes were kindly gifted by Dr. Akiyoshi Uemura. The images were observed under a Keyence BZ-X700 microscope.

Wound healing assay

LECs (cc-2810, Lonza) were grown to confluence in EGM2 medium (cc-3162, Lonza) supplemented with 15% fetal bovine serum (FBS), and then shifted to LEC medium lacking growth factors and containing 0.5% FBS for 16 h. The confluent LECs were wounded using 1000-μL pipette tips. The remaining cells were washed twice with PBS to remove cell debris and then incubated in EGM2 medium supplemented with 15% FBS with PBS or Sema3E (3239-S3, R&D) for an additional 48 h. The images were observed under a Keyence BZ-X700 microscope, and the wound size was evaluated using NIH ImageJ.

LEC proliferation assays

LECs were seeded (5×10^4 cells/well) in 0.2% gelatin-coated 96-well plates and incubated for 24 h in EGM2 medium supplemented with 15% FBS. Then, the medium and/or Sema3E was added and incubated for an additional 48 h. The number of cells was determined using Cell Count Kit-8 (Doujindo, Kumamoto, Japan) and measured using a fluorescence spectrometer equipped with a microplate reader.

Phosphorylation assay

LECs were grown to confluence in growth medium and then shifted to medium lacking growth factors and containing 0.5% FBS for 16 h. Then, the cells were incubated with PBS or Sema3E (10 nM) for 2 h, followed by stimulation with VEGF-C (200 ng/mL). ERK1/2 and AKT phosphorylation was determined by western blotting.

Generation of expression vectors

To generate the pFLAG-T2A-EGFP vector, sequences corresponding to the picornavirus T2A and enhanced green fluorescent protein (EGFP) were inserted into the multiple-cloning site (MCS) of pFLAG-CMV2 (Sigma). The sequence for human Sema3E was also inserted into the MCS located before T2A of pFLAG-T2A-EGFP to generate pFLAG-Sema3E-T2A-EGFP. The constructs were verified by sequencing.

siRNA transfection

LECs were seeded in 0.2% gelatin-coated 6-well dishes at a concentration of 9×10^5 cells/well

in EGM2 medium supplemented with 15% FBS. The following day, cells were transfected with siControl (Invitrogen, medium GC duplex, 462001) or siPlexinD1 (Invitrogen, HS118222-4) using Lipofectamine RNAiMax transfection reagent (Invitrogen, 13778150) according to the manufacturer's instructions. The efficiency of siPlexinD1 was determined by western blotting. The sequences of siRNAs are shown in Table 2.

LEC repulsive assays

HLECs were cultured to 30-40% confluency. The following day, up to 2×10^2 HEK-293T cells transfected with pFLAG-T2A-EGFP or pFLAG-Sema3E-T2A-EGFP were seeded on top of LECs and incubated for an additional 48 h. For actin staining, cells were fixed with 4% PFA and incubated with Acti-stain 555 fluorescent phalloidin (Cytoskeleton) and GFP antibody (Nacalai Tesque), followed by incubation with secondary antibodies for GFP and DAPI for nuclear staining. Untreated LECs were used for time-lapse images, which were obtained every 10 min to 72 h using a confocal laser-scanning microscope (FluoView FV10i, Olympus). The obtained images were processed with FLUOVIEW (Olympus) and NIH ImageJ.

LEC spheroid sprouting assay

LECs were seeded in 0.2% gelatin-coated 6-well dishes at a concentration of 8×10^5 cells/well in EGM2 medium supplemented with 15% FBS. The following day, 1.2×10^6 LECs were mixed with EGM2 medium containing 0.24% methylcellulose (Sigma) and allowed to aggregate in round-bottom 96-well plates for 12 to 24 h (3000 cells per spheroids). The spheroids were subsequently embedded in type1 collagen (Nitta Gelatin, Osaka, Japan) and incubated for an additional 48 h. Then, spheroids were fixed in 4% PFA and incubated with fluorescent-labeled phalloidin (Cytoskeleton) and GFP antibody (Nacalai Tesque), followed by incubation with secondary antibody for GFP and DAPI for nuclear staining. Images were observed under a Keyence BZ-X700 microscope.

Murine cardiac injury model

Eight to twelve-week-old C57BL/6N male mice, weighing 22–27 g, underwent surgery. The mice were anesthetized with pentobarbital at 30 mg/kg for induction and 1.5-4.0% isoflurane for maintenance and were placed under assisted external ventilation after tracheal intubation. Cardiac injury was induced via permanent ligation of the left descending artery (LAD) at the medial location of the heart using a 10-0 ligature, and ST changes in the limb lead were monitored. Then, mice were randomly allocated to groups that received intraperitoneal injections of 0.1 μg/g recombinant PlexinD1 (4160-PD, R&D Systems) and PBS as a control.

Further injections were administered on days 2, 3, 4, and 6 post-surgery. The experimenters were double blinded to treatment and control assignments. The sample size was estimated using G*power (http://www.gpower.hhu.de/), and mice that died within 30 min of surgery were excluded from analyses as death due to surgery. Mice hearts were collected at 28 days post-MI and were either sectioned for histology and immunofluorescence staining or prepared for protein extraction. The mice were housed and maintained in a controlled environment.

Echocardiography

Echocardiography was performed in mice sedated with isoflurane, as previously described (Matsuura et al., 2009). Transthoracic echocardiography was performed using a Nemio 35 ultrasound system (Toshiba), with a 12-MHz imaging transducer, and the heart rate was maintained at approximately 500 bpm by adjusting the concentration of isoflurane to minimize data deviations during cardiac function measurements.

Western blotting

Total protein extract was obtained by lysing cells and the injured left ventricles of the MI hearts in RIPA buffer [150 mM NaCl, 0.1% Triton X-100, 0.5% Sodium deoxycholate, 0.1% SDS, 50 mM Tris-HCl (pH 7.6) supplemented with 25 mM NaF, 1 mM Na3VO4 and protein inhibitor cocktail (11873580001, Roche)]. Protein concentrations were quantified using DC protein assay kits (Bio-Rad). After equal amounts of proteins were loaded and separated via SDS–PAGE, the proteins were transferred to PVDF membranes (Immobilon-P, Millipore), blocked with 0.3% milk/TBST and incubated with primary antibodies against Sema3E (ab112886, Abcam, 1:10,000), VEGFR3 (AF743, R&D Systems, 1:5,000), β-Actin (sc-47778, Santa Cruz Biotechnology, 1:20,000), HPRT (GTX113466, GeneTex, 1:2,000), phospho-Erk (9106, Cell Signaling Technology, 1:1000), phospho-Akt (9271, Cell Signaling Technology, 1:1000), Akt (9272, Cell Signaling Technology, 1:1000), Erk (9102, Cell Signaling Technology, 1:1000), or PlexinD1 (AF4160, R&D Systems, 1:2,000) overnight at 4 °C. Then, membranes were incubated with horseradish peroxidase (HRP)-conjugated secondary antibodies (ab97110 or ab6721, Abcam, 1:5,000) for 1 h at room temperature. The proteins were detected using an ImageQuant LAS 4000 instrument (GE Healthcare).

Histological assessment of fibrosis

Serial 4 μm transverse paraffin sections of MI hearts were stained with Masson's trichrome solution and images were captured using a Keyence BZ-X700 microscope to quantify cardiac fibrosis. Using ImageJ software, the extent of fibrosis in sections was quantified as the relative

area of positive Masson's trichrome-stained area (blue fibrosis) normalized to the total section area.

Statistical analysis

Data are presented as the mean ± standard error of the mean (SEM). One-way analysis of variance (ANOVA) followed by Bonferroni's test was applied to multiple-group comparisons. Mann-Whitney's *u*-tests were applied to two-group comparisons. *P*-values less than 0.05 were considered statistically significant.

REFERENCES

Asai, R., Kurihara, Y., Fujisawa, K., Sato, T., Kawamura, Y., Kokubo, H., Tonami, K., Nishiyama, K., Uchijima, Y., Miyagawa-Tomita, S., Kurihara, H., 2010. Endothelin receptor type A expression defines a distinct cardiac subdomain within the heart field and is later implicated in chamber myocardium formation. Dev Camb Engl 137, 3823–33. https://doi.org/10.1242/dev.054015

Gu, C., Yoshida, Y., Livet, J., Reimert, D.V., Mann, F., Merte, J., Henderson, C.E., Jessell, T.M., Kolodkin, A.L., Ginty, D.D., 2005. Semaphorin 3E and Plexin-D1 Control Vascular Pattern Independently of Neuropilins. Science 307, 265–268. https://doi.org/10.1126/science.1105416

Matsuura, K., Honda, A., Nagai, T., Fukushima, N., Iwanaga, K., Tokunaga, M., Shimizu, T., Okano, T., Kasanuki, H., Hagiwara, N., Komuro, I., 2009. Transplantation of cardiac progenitor cells ameliorates cardiac dysfunction after myocardial infarction in mice. J Clin Invest 119, 2204–17. https://doi.org/10.1172/jci37456

Zudaire, E., Gambardella, L., Kurcz, C., Vermeren, S., 2011. A Computational Tool for Quantitative Analysis of Vascular Networks. Plos One 6, e27385. https://doi.org/10.1371/journal.pone.0027385

	Forward(5'-3')	Reverse(5'-3')
Sema3E KO	GACAGAAAGGCTTAGCGGATC	CTTGCTCACCATGGTGCGTG
Sema3E WT	GACAGAAAGGCTTAGCGGATC	GGTTCGCCGAGTGACCTG
PlxnD1 KO	ATGGTGAGCAAGGGCGAGGA	TTACTTGTACAGCTCGTCCA
PlxnD1 WT	ACCGCAGAACCGGTCACCGTGTT	GGTTAAGGTCGAAGGTGAAGAGCTT

Table 1. Primers used for genotyping.

Table 1, related to Figure1-5

	(5'-3')
siPlexinD1#1	GGAGGCUUCUCAAGAUCAACCUGAA
siPlexinD1#2	UGUUCCCGCUCAGCCUCCAACUAAA
siPlexinD1#3	GGGAAUUAGCUUGUUCUCCUCACUA

Table 2. The sequences of siPlexinD1

Table 2, related to Figure 6